JGR Planets

RESEARCH ARTICLE
10.1029/2022JE007320

Key Points:

- Spectral and morphologic analyses highlight multiple events related to water activity within Becquerel crater
- Widespread faulting suggests the internal collapse of a layered mound, possibly due to fluid expulsion from below
- Differences in elevation reflect different mineralogies and layer thicknesses between two layered deposits

Supporting Information:

Supporting Information may be found in the online version of this article.

Correspondence to:

G. Schmidt,
genewalter.schmidt@uniroma3.it

Citation:

Schmidt, G., Luzzi, E., Rossi, A. P., Pondrelli, M., Apuzzo, A., & Salvini, F. (2022). Protracted hydrogeological activity in Arabia Terra, Mars: Evidence from the structure and mineralogy of the layered deposits of Becquerel crater. *Journal of Geophysical Research: Planets*, *127*, e2022JE007320. https://doi.org/10.1029/2022JE007320

Received 30 MAR 2022
Accepted 30 AUG 2022

Author Contributions:

Conceptualization: G. Schmidt, E. Luzzi, A. P. Rossi, A. Apuzzo, F. Salvini
Data curation: G. Schmidt, E. Luzzi, A. P. Rossi
Formal analysis: G. Schmidt, E. Luzzi, M. Pondrelli
Funding acquisition: F. Salvini
Investigation: G. Schmidt, E. Luzzi, M. Pondrelli
Methodology: G. Schmidt, E. Luzzi, A. P. Rossi, M. Pondrelli, F. Salvini
Project Administration: G. Schmidt
Resources: G. Schmidt, A. P. Rossi
Software: F. Salvini

Protracted Hydrogeological Activity in Arabia Terra, Mars: Evidence From the Structure and Mineralogy of the Layered Deposits of Becquerel Crater

G. Schmidt[1], E. Luzzi[2], A. P. Rossi[2], M. Pondrelli[3], A. Apuzzo[1], and F. Salvini[1]

[1]Department of Science, Università degli Studi Roma Tre, Rome, Italy, [2]Department of Physics and Earth Sciences, Jacobs University Bremen, Bremen, Germany, [3]International Research School of Planetary Sciences, Università d'Annunzio, Pescara, Italy

Abstract The formation of layered mounds on Mars remains a major topic of debate, with the relationship between their deposition and chemical alteration a major aspect still to be constrained. The association these deposits have with hydrated minerals indicates aqueous processes were active in their past, however the extent and duration of this aqueous period has yet to be fully realized. We studied compositional, stratigraphical, and structural characteristics of two separate layered deposits within Becquerel crater, Arabia Terra, to constrain their origins and the intensity of past aqueous activity. We find that due to key differences in composition, layering, and deformation between the two deposits, the timing of important depositional changes within Becquerel can be identified. We propose a scenario involving differences in fluid expulsion intensity and water level between the two layered deposits, in which diverse depositional and post-depositional environments were able to form. Furthermore, internal collapsing and deformation of the main mound might reflect that fluid upwelling persisted below the mound after formation. Determining the relationship between these two deposits is an important step in unraveling the past climate of Arabia Terra, and more broadly Mars. The evidence of protracted fluid expulsion represents a unique opportunity for future missions searching for signs of past life.

Plain Language Summary Becquerel crater is located in the Arabia Terra region (Mars), and it is characterized by the occurrence of a large layered mound. We used spectral reflectance to study mineralogy within the layered mound, finding hydrated sulfates, minerals which formed in the presence of water. In addition, we noticed that not far from the mound, there are separate layered deposits within a smaller interior crater on the floor of Becquerel crater. This interior crater creates nearly a kilometer difference in elevation between the large layered mound and the separate layered deposits, leaving the separate layered deposits mostly isolated from the rest of Becquerel. The layered deposits within the interior crater were found to have unique clay lithologies. We compared these separate layered deposits with those of the large layered mound to determine their relationship and we concluded that their origins might be related to fluid expulsion which exploited weak areas of the crater floor from the intersections of impact related radial faults and a pre-existing regional fault. Due to the abundance of fluvial related structures and hydrated mineral assemblages, Becquerel might be considered an optimal place to search for signs of past life.

1. Introduction

The presence of water-altered sedimentary rocks and past aqueous depositional environments on Mars have been substantiated by both orbital and surface instrumentation (Carr & Head, 2010; Changela et al., 2022; Malin & Edgett, 2000). High-resolution orbital images combined with rover and lander images have shown distinct sedimentary layers ranging from scales of meters to millimeters in thickness (Annex & Lewis, 2020; Deit et al., 2013; Fueten et al., 2014; Grotzinger et al., 2014; Lewis & Aharonson, 2014; Lewis et al., 2008; Rampe et al., 2017; Salese et al., 2020; Schmidt et al., 2018, 2021; Thomson et al., 2011; Wray, 2013). One specific type of layered material, often called equatorial layered deposits (ELDs), occurs in many craters and basins, and has been interpreted as forming from various depositional processes including lacustrine (Day et al., 2019; Lucchitta, 2010; Lucchitta et al., 1992), aeolian (Annex & Lewis, 2020; Kite et al., 2013; Lewis & Aharonson, 2014), mud volcanism (Pondrelli et al., 2011), spring and/or evaporitic (Allen & Oehler, 2008; Andrews-Hanna et al., 2010; Franchi et al., 2014; Pondrelli et al., 2015, 2019; Pozzobon et al., 2019; Rossi et al., 2008), as well as mixed processes within changing depositional environments (Day et al., 2019;

Supervision: G. Schmidt, A. P. Rossi, F. Salvini
Validation: G. Schmidt, A. P. Rossi
Visualization: G. Schmidt, F. Salvini
Writing – original draft: G. Schmidt, E. Luzzi, A. P. Rossi, M. Pondrelli, A. Apuzzo, F. Salvini
Writing – review & editing: G. Schmidt, E. Luzzi, A. P. Rossi, M. Pondrelli, A. Apuzzo, F. Salvini

Schmidt et al., 2021). Apart from the depositional interpretation, the importance of groundwater in the ELDs emplacement and preservation has been previously hypothesized by many including Andrews-Hanna et al. (2007, 2010), Franchi et al. (2014), and Oehler and Allen (2010), Pondrelli et al. (2015), Rossi et al. (2008), Salese et al. (2019), Schmidt et al. (2021), and Zabrusky et al. (2012). ELDs occur in a range of sizes and shapes (Annex & Lewis, 2020; Schmidt et al., 2021), from massive kilometer tall mounds (Day & Catling, 2020; Franchi et al., 2014) to meter-scale packages (Pondrelli et al., 2019; Pozzobon et al., 2019; Schmidt et al., 2021). Imaging spectrometer instruments have detected a variety of hydrated minerals in direct association (i.e., on the surface or amongst layering), and within the localities, of these layered deposits and include phyllosilicates and sulfates (Flahaut et al., 2015; Gendrin et al., 2005; Michalski et al., 2019; Milliken et al., 2010; Murchie et al., 2009; Poulet et al., 2008; Squyres, Arvidson, et al., 2004; Squyres, Grotzinger, et al., 2004; Zabrusky et al., 2012). These minerals form in stable hydrological systems and indicate distinct depositional environments once existed (Carter et al., 2013). Thus, the presence of these minerals indicates that water was present during ELD evolution, either during deposition or post-deposition (Schmidt et al., 2021). The duration of water activity within these environments may have been either a relatively brief (Koeppel et al., 2022) or prolonged (Andrews-Hanna et al., 2007, 2010; Di Pietro et al., 2018; Salese et al., 2019) period in Martian geologic history.

A majority of the ELDs are found in the broad equatorial region called Arabia Terra (Annex & Lewis, 2020; Day & Catling, 2020; Schmidt et al., 2021). This region spans nearly 5,000 km along the transition zone between the northern lowlands and the southern highlands. Arabia Terra bears evidence of groundwater activity (Andrews-Hanna et al., 2007, 2010), the existence of deltas (Salese et al., 2019), a potential ocean shoreline (Baker et al., 1991; Di Achille & Hynek, 2010; Rodriguez et al., 2016; Webb, 2004), outflow channels (Fawdon et al., 2022; Molina et al., 2017) volcanic activity (Michalski & Bleacher, 2013; Whelley et al., 2021), and vast deposits of hydrated minerals (Bishop et al., 2020; Gou et al., 2014; Loizeau et al., 2010, 2012, 2015; Michalski, Cuadros, et al., 2013, 2019; Noe Dobrea et al., 2011; Wray et al., 2008). In the west, at the location of the potential shoreline, a region of Arabia Terra called Oxia Planum is the selected landing site of the ExoMars 2022 rover due to a variety of fluvial features and hydrated mineral detections (Lakdawalla, 2019; Quantin-Nataf et al., 2021; Vago et al., 2015, 2017). Murchie et al. (2009) recognized monohydrated and polyhydrated sulfate signatures in association with ferric minerals typical of the aeolian dust on Mars. This association has been thought to involve both evaporitic and aeolian processes, whose alternation would have been caused by fluctuations of a regional groundwater table (Andrews-Hanna et al., 2007, 2010). Poulet et al. (2008) suggested that sulfates and phyllosilicates in Arabia Terra represent two separate formation events driven by different processes. Unfortunately due to the widespread occurrence of dust (Andrews-Hanna et al., 2010; Mangold et al., 2009), the orbital spectrometer data sets (Compact Reconnaissance Imaging Spectrometer for Mars [CRISM] and the Observatoire pour la Minéralogie, l'Eau, les Glaces et l'Activité [OMEGA]) are not always effective in Arabia Terra. In the south, it borders Merdiani Planum, where the Opportunity Rover analyzed a plethora of hydrated minerals and famously discovered hematite spherules thought to be formed by groundwater (McLennan et al., 2005; Squyres, Arvidson, et al., 2004; Squyres, Grotzinger, et al., 2004). Due to the wide variety of fluvial morphologies and sedimentary structures across the region, classifying the surface composition in Arabia Terra has become an important aspect of determining past climates on Mars. Since these ELDs encompass many of these morphologies, structures, and minerals, classifying each ELD in Arabia Terra can therefore help constrain Martian climate evolution.

Apart from the morphological, sedimentological, and compositional aspects of the ELDs in Arabia Terra, structural features (i.e., tilted layering, faults, and deformational features) can describe their depositional and post-depositional history (Annex & Lewis, 2020; Fueten et al., 2005, 2008, 2014, 2017; Schmidt et al., 2018, 2021). Specifically, categorizing layer attitudes between syndepositional and post-depositional features could help constrain layer formation (Annex & Lewis, 2020; Kite et al., 2013; Schmidt et al., 2018). Regional compressional tectonic structures recognized in Arabia Terra include wrinkle ridges perpendicular to the Martian dichotomy and lobate scarps roughly parallel to the dichotomy and interpreted as the surface evidence of buried thrust faults (Golombek et al., 2001; McGill, 2000; Watters, 2003). In addition, gentle folds were recognized deforming the layered deposits (Franchi et al., 2014; Murana, 2018, Schmidt et al., 2021). The extensional structures are represented by grabens (Anderson et al., 2008) and minor extensional faults affecting the layered deposits inside the craters (Murana, 2018; Pondrelli et al., 2011, 2015). Strike-slip structures were also identified within the craters by Rossi et al. (2009) and Murana (2018). The occurrence of deformation bands in Arabia Terra was proposed by Okubo et al. (2009), who also described the diagenetic processes that may have influenced the layered deposits.

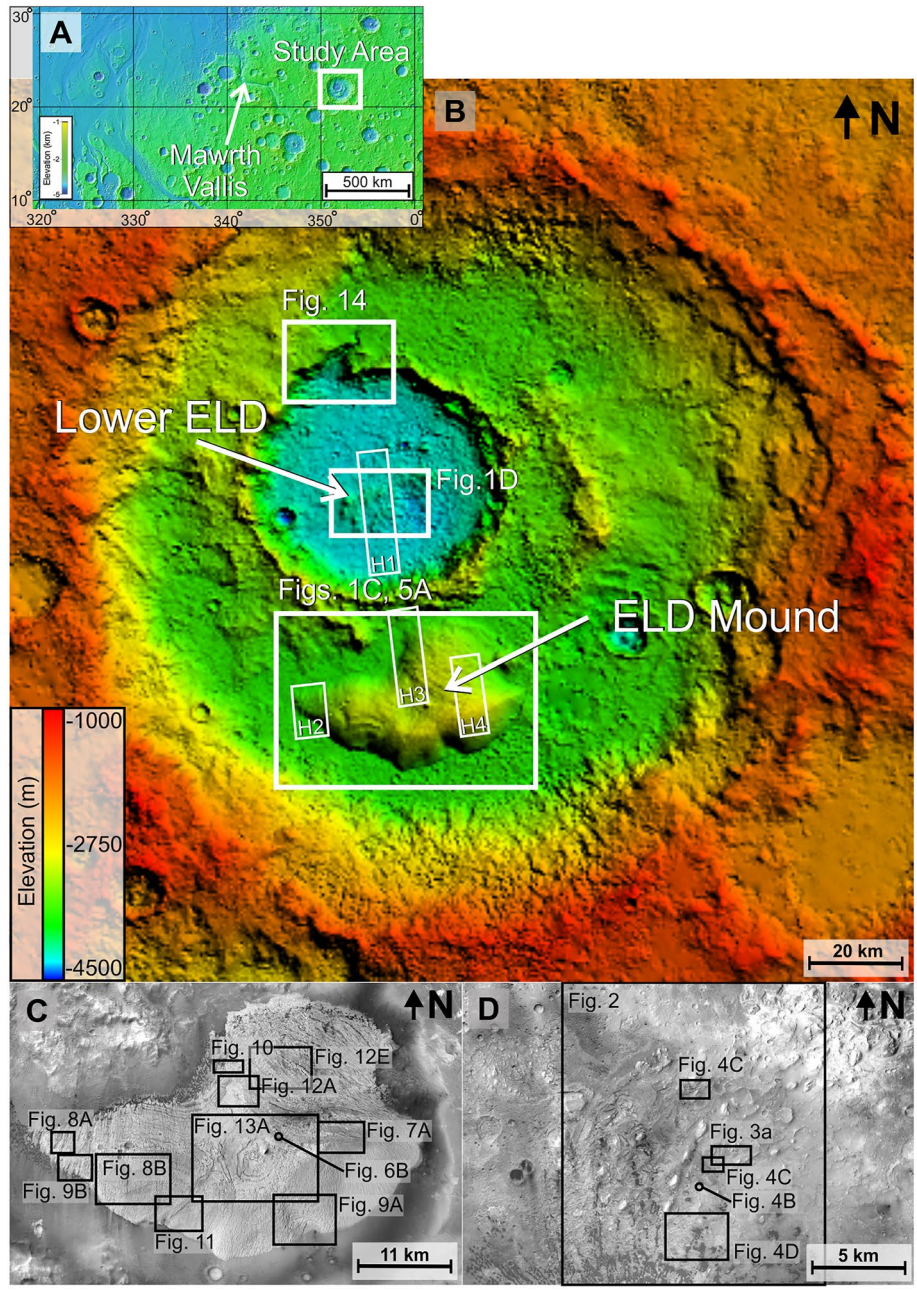

Figure 1. (a) Location of Becquerel crater on a Mars Orbiter Laser Altimeter (MOLA) elevation basemap. (b) High Resolution Stereo Camera composite digital elevation model (DEM) of Becquerel crater showing the locations of the equatorial layered deposit (ELD) Mound and the Lower ELD located in a second large crater on the floor of Becquerel crater. Footprints of HiRISE DEMs are labeled H1-H4. H1 = ESP_025782_2020/ESP_025637_2020, H2 = ESP_034419_2015/ESP_033707_2015, H3 = PSP_001546_2015/PSP_001955_2015, H4: PSP_003656_2015 PSP_005845_2015. (c) CTX image of the ELD Mound. (d) CTX image of the Lower ELD. CTX images G19_025782_2021, P12_005845_2021, and P19_008495_2015.

Becquerel crater is a large basin within Arabia Terra (Figure 1). It is unique to other ELD bearing craters in Arabia Terra because it contains two distinct ELDs: a large mound and a smaller sized deposit. The large mound might represent the highest latitude ELD mound observed on Mars (Day & Catling, 2020; Schmidt et al., 2021). In this study these two ELDs were determined to be completely isolated from each other by the presence of an interior crater within Becquerel, a unique setting for an ELD not observed elsewhere on Mars to date. Consequently, they differ in size, mineralogy, layer thickness, layer attitude, and deformation, which indicates a complicated

depositional regime during periods of changing water level. Structural differences between the ELDs, accompanied with specific mineralogies at lower elevations, suggest that hydrothermal processes were present after their formation. These findings contribute to the advancement of stratigraphic correlations of ELDs across Mars and contribute to the identification of climate change markers. Furthermore, investigation of Becquerel will further constrain and catalog locations on the surface of Mars that have the potential of hosting evidence of past microbial life.

2. Geological Setting and Previous Work

Becquerel is a large 165 km diameter, 4.3 km deep, crater located in northwestern Arabia Terra and centered at 21.89°N, 352.06°E (Figure 1). The surrounding area is mostly Noachian in age, with the exception of Hesperian-Amazonian aged sedimentary deposits and impact craters (Tanaka et al., 2014). The area contains several wrinkle ridges and outflow channels, including the large meandering outflow channel called Mawrth Vallis (Tanaka et al., 2014), located 280 km west of Becquerel (Figure 1a). Mawrth Vallis is well known for an abundance of both hydrated sulfates and clays within unique sedimentary successions (Bishop et al., 2008, 2020; Loizeau et al., 2010, 2012, 2015; Noe Dobrea et al., 2011; Wray et al., 2008) and was a top candidate landing site for both the Mars Science Laboratory (Golombek et al., 2011; Grant et al., 2011) and ExoMars (Westall et al., 2014). Moving further westward from Becquerel, the regional elevation decreases a full kilometer from approximately −2,700 m to −3,700 m, before ending at the potential shoreline of an ancient ocean (Di Achille & Hynek, 2010; Rodriguez et al., 2016; Webb, 2004). The impact event which formed Becquerel is considered to be Late Noachian (Tanaka et al., 2014).

Becquerel is distinct among other craters in the region due to its isolated layered mound and a separate layered deposit located in an interior crater (henceforth referred to as the ELD Mound and the Lower ELD). Like other massive layered deposits, these ELDs are thought to have formed in Early-Middle Hesperian time (Carr & Head, 2010; Lewis & Aharonson, 2014; Lucchitta et al., 1994; Schultz, 1998).

The ELD Mound is located within the southern area of the crater (Figure 1c) and hosts many stratigraphic and structural features (described in Section 4 Results). It has previously been interpreted in a variety of depositional settings including lacustrine and playa environments due to the oscillations of the groundwater table (Andrews-Hanna et al., 2010; Rossi et al., 2009), diapirism (Popa et al., 2008), glacial accumulation (Bridges et al., 2008), alkaline lacustrine environment (Crowley et al., 2008) and lacustrine/aeolian deposition (Cadieux & Kah, 2015), possibly driven by cyclic controls on deposition (Lewis & Aharonson, 2014; Lewis et al., 2008). Additionally, Urso et al. (2018) described the interactions between dunes and yardangs associated with the ELDs in an effort to constrain the modern sedimentary transport within Becquerel.

The Lower ELD is located 30 km north of the ELD Mound within an interior crater at an elevation 700 m lower than the surrounding floor of Becquerel (Figure 1d). Schmidt et al. (2021) demonstrated that the craters Becquerel and nearby Trouvelot might represent a facies change. This was due to a regional layer thickness change from thicker layering in the southeast to thinner layering in the northwest, with −1,400 m elevation being a major boundary. Since this elevation passes between the Lower ELD and the ELD Mound, it was suggested that Becquerel might be a focal point of the facies change. Specifically, the thicker ELDs to the southeast (Annex & Lewis, 2020; Pondrelli et al., 2019) and the ELD Mound might share a similar source or formation. Likewise, the Lower ELD might be considered similar to the thinner clay dominated deposits to the northwest (Michalski, Niles, et al., 2013, 2019; Wray et al., 2008).

The previous work in Becquerel mostly revolves around the ongoing question of how water played a role in sediment deposition on Mars and to what extent. Layering sequences in the ELD Mound were first identified by Lewis et al. (2008) and proposed to correlate to the obliquity cycle of Mars. They calculated that the depositional rate was 3×10^{-5} m/year (Lewis et al., 2008) which was then used to support a calculated groundwater upwelling rate of 10^{-3} m/year in Becquerel (Andrews-Hanna et al., 2010). Bridges et al. (2008) pointed out the similarity between the ELD Mound and the Polar Layered Deposits. A deposition also based on obliquity cycles was invoked, but in the added context of sublimating seasonal frost/ice that leaves behind layers of dust. Rossi et al. (2009) proposed the ELD Mound to be similar to travertine in an environment of emerging subsurface fluid. This was based on both sedimentary structures and mound architecture. Based on the interpretation of large-scale movements of material on all sides of the mound, Popa et al. (2008) proposed that a salt glacier (or namakier)

resulting from diapirism underneath the mound was responsible for the observed layering and structure. Crowley et al. (2008) also noticed the layered sequences, but suggested the existence of an alkaline lake due to the lack of hydrated minerals detected in the study. Cadieux and Kah (2015) pushed the geological interpretation of Becquerel to its furthest extent by measuring depositional couplets (i.e., beds) and elaborating on the importance of accommodation space as a control. Although no specific depositional process was proposed, they suggested that the process was likely a mixed lacustrine/aeolian environment in which sediment deposition was controlled by the fluctuation of the water level possibly controlled by groundwater. Our study improves upon these works by incorporating the Lower ELD and other sedimentary structures within the interior crater. We also provide updated layer thickness measurements which expand the observed stratigraphy of Becquerel which has previously only focused on the ELD Mound. Additionally, detailed spectral and structural analyses lead to better constraints on the types of possible water activity that occurred. Thus, our work provides a new perspective of Becquerel in unprecedented detail. The understanding of the depositional environment that was present in Becquerel is improved, and a detailed sequence of events can be extracted from these new observations and analyses.

3. Data and Methods

3.1. Image Data

We utilized a variety of orbital data sets in order to measure layering and map faults in an effort to distinguish the characteristics of the Lower ELD and ELD Mound. The image data sets used in this study are a combination of HiRISE (High Resolution Imaging Science Experiment, image: 0.30 m/px, DEM: 0.4–0.6 m/px) (McEwen et al., 2007), CTX (Context Camera, image: 6.0 m/px, DEM: 6.2 m/px) (Malin et al., 2007), and HRSC (High Resolution Stereo Camera, DEM: 50.0 m/px) (Jaumann et al., 2007; Neukum & Jaumann, 2004). We used a CTX mosaic for broad observations and specific stereo pairs of HiRISE and CTX to create digital elevation models (DEMs). We then used the DEMs for 3D viewing and layer measurements. An HRSC DEM was used as a base layer for the entire study. We processed the images by means of the software ISIS 3 (Integrated Software for Imagers and Spectrometers), developed by the USGS. HiRISE and CTX DEMs were produced through the NASA Ames Stereo Pipeline (Beyer et al., 2018; Moratto et al., 2010). We then integrated the data into the GIS software Global Mapper v15.2 (Blue Marble Geographics, 2011) using an equirectangular projection where the stereo pair derived DEMs were tied to the base HRSC DEM. All data are listed and categorized in Table S1 of Supporting Information S1.

3.2. VNIR Spectral Data

In order to determine possible differences in the depositional environments between the Lower ELD and ELD Mound, we identified minerals through rudimentary spectral analyses using hyperspectral data from the CRISM instrument. We focused on spectral features in the near infrared to determine the presence of water-alteration and infer what types of mineral assemblages best describe the acquired spectra (Murchie et al., 2007, 2009). To assess the extent of the hydrated mineralogy and identify specific areas of mineral types, we created two spectral parameter maps using three full resolution observations (FRT, 18 m/pixel) and two half resolution observations (HRL, 36 m/pixel). We used the CRISM Analysis Tool (CAT) package available in the Environment for the Visualization of Images (ENVI) (Murchie et al., 2009), following the method described by Flahaut et al. (2015). Both the photometric correction and volcano-scan atmospheric correction methods (McGuire et al., 2009; Murchie et al., 2007) available in CAT were used in all the presented ratioed spectra.

Spectral parameters from Viviano-Beck et al. (2014) were used to assess and present absorptions specific to certain minerals. We identified the minerals by observing the overtones and fundamental vibrational absorption features in the 1.0–2.6 μm interval, where CRISM can identify hydrated minerals (e.g., Clark, King, et al., 1990; Clark, Swayze, et al., 1990; Flahaut et al., 2015; Gendrin et al., 2005; Hunt, 1970). A key indication of the presence of water is the absorption near 1.9 μm caused by combination vibration of H_2O (Bishop et al., 1994; Burns & Fisher, 1993; Clark, King, et al., 1990; Clark, Swayze, et al., 1990). Thus, this absorption is a key feature in all the presented spectra. We manually examined individual pixels for relevant signatures and then grouped them into regions of interest (ROI). The ratioed spectra presented are averages of tens of pixels from nine chosen ROIs divided by the averages of neutral spectra ROIs which were taken from the same detector columns. However, due to noise we were forced to ratio the ROI labeled #9 by using neutral spectra from an area outside of the ROI's detector columns. The unratioed and neutral spectra are presented in Supporting Information S1. We compared the ratioed spectra to terrestrial reference spectra from the CAT (Kokaly et al., 2017; Murchie et al., 2007)

spectral library for mineral identification. Arabia Terra is known for particularly high dust coverage (Mangold et al., 2009). Due to substantial dust cover collected on the ELD Mound, there are many places where dust interference impeded the extraction of reliable spectra. Despite this, the presented ROIs represent areas where absorptions were determined to be unhindered by dust. Conversely, the Lower ELD within the interior crater is relatively dust free and thus the full-resolution targeted observation available yielded more pristine spectra.

3.3. Layer Measurements

Using DEMs derived from the four HiRISE stereo pairs (Figure 1b), we measured layer thicknesses in both the Lower ELD and the ELD Mound. We then determined layer thicknesses by measuring elevation and distance between each layer following the methodology of Schmidt et al. (2018, 2021) and Fueten et al. (2008, 2014). The resulting measurements had an estimated error of ±0.4 m due to both vertical precision of the DEMs (generally <0.5 m) (McEwen et al., 2007; Sutton et al., 2015), and erosion of the layer edges (Annex & Lewis, 2020; Schmidt et al., 2021). To reduce error, all DEMs used were geometrically corrected to ensure vertical precision and careful selection of both transects and point placement. Points were placed on layer edges along transects parallel to the dip direction (Schmidt et al., 2021). The elevation difference of the two points was then a value for the layer thickness. Careful attention to point placement was given using 3D scenes to ensure points were not placed on erosional surfaces (Annex & Lewis, 2020; Fueten et al., 2014; Schmidt et al., 2021). When necessary, dips were corrected for by multiplying the tangent of the dip angle by the horizontal distance between two adjacent layer edges, and then subtracting the vertical distance between the two layer edges (Schmidt et al., 2021). A total of 271 layers were measured along 27 transects. In order to better visualize thickening and thinning sequences, we averaged layer thicknesses (Schmidt et al., 2018, 2021) in groups of 50 m vertical sections. We repeated this by advancing this averaging upwards in elevation every 10 m. These values were then placed into graphs as trendlines superimposed on the unaveraged layer thickness values so that the general layer thickness changes within the stratigraphic succession of the ELDs could be identified.

We obtained layer attitudes from DEMs derived from the four HiRISE stereo pairs and one CTX stereo pair (Table S1 in Supporting Information S1) by using the Orion software (Pangaea Scientific, 2011). Orion is a structural analysis software with internal operations and functionality established in Fueten et al. (2005, 2006, 2008). Over the last decade Orion has been used extensively across Mars for developing the structural framework of the layered deposits of Valles Marineris (Fueten et al., 2010, 2011, 2014, 2017; Okubo, 2014; Schmidt et al., 2018), western Arabia Terra (Pondrelli et al., 2015, 2019; Schmidt et al., 2021), and Gale Crater (Deit et al., 2013). The procedure of measuring layer attitudes begins by placing a series of continuous points along the edge of a layer and calculating the best-fit three-dimensional plane. Point spacing can vary 20–100 m and a series can measure 500–2,000 m in length. Sets of points were repeatedly placed laterally across layering to determine where layers change attitude and to ensure that the transects used for measuring layer thickness can be accurately placed. Sets had an average of seven points. Each set produced a dip measurement with an error always less than the dip value and with an average dip error of 3°. We computed 107 layer attitudes from the ELDs and 39 layer attitudes from nearby layered fan-shaped deposits.

3.4. Evaluating Depositional Processes

We have compared the viability of all possible depositional processes and settings by assessing which of our observations could have been produced by them. This was achieved by creating a complete catalog of the possible depositional processes, our observations, and the implications each process would have in Becquerel (Tables 1 and 2). This produces an in depth review of layer deposition and depositional environments on Mars and how they can be framed within Becquerel.

4. Results

4.1. Lower ELD

The Lower ELD is well exposed, covering a surface area of approximately 215 km^2 within the central area of the interior crater (Figures 1 and 2a). It has a total volume of approximately 6.21 km^3, yet a highly variable total thickness ranging 50–250 m. It is characterized by the presence of two distinct spectral signatures, thin layers, truncated layered sections, areas of relatively high layer attitude, linear ridges, and minor faulting. Furthermore, it is located in the lowest elevation of Becquerel at approximately −4,400 m.

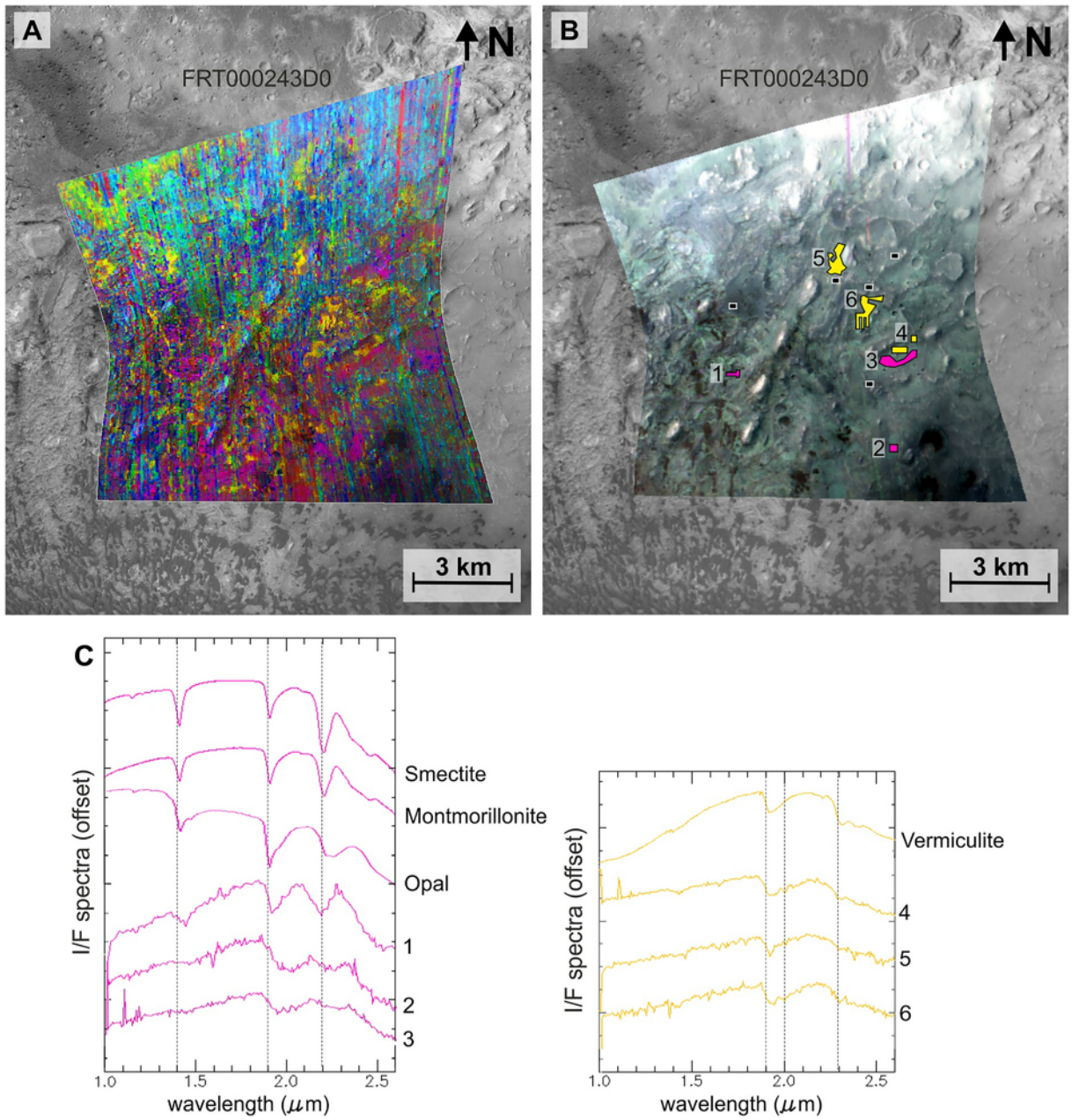

Figure 2. Compact Reconnaissance Imaging Spectrometer for Mars (CRISM) analysis of the lower equatorial layered deposit. (a) CRISM RGB composite of observation FRT000243D0 projected over a CTX mosaic. Summary parameters highlighting hydrated mineral detections (R = BD1900_2 [0.0–0.044], G = BD2290 [0.0–0.017], B = SINDEX2 [0.0–0.031]). (b) False color composite. The colored polygons indicate the locations of pixels used to obtain the spectra 1–6. The black squares indicate the locations used as a common denominator for ratios. (c) Six separate ratioed spectra identified in FRT000243D0. Spectra 1–3 and 4–6 are grouped together and placed into separate graphs based on similar absorptions and waveform. Vertical bars are placed at specific absorptions for clarity. Spectrum 1 ratio is the "median" option display in ENVI (see Supporting Information S1 for "normal" display). Library spectra; smectite BKR1JB005, montmorillonite 0397S013, opal TM8896, and vermiculite LAVE01.

A detailed CRISM analysis involving six ROIs led us to establish two distinct and reoccurring hydrated mineral signatures within the Lower ELD (Figure 2). These two signatures are distinct from each other due to differences in the width of absorption between 1.90 and 2.00 μm and more specific absorptions between 2.20–2.25 and 2.29 μm (Figure 2c). These two signatures were not detected in the ELD Mound and are consistently associated with specific morphologies (i.e., layered and non-layered) (Figure 3). The first signature type has a strong absorption at 1.9 μm and a broad absorption between 2.20 and 2.25 μm (Figure 2c, spectra 1, 2, and 3 in left column). There is faint evidence of a weak absorption between 1.40 and 1.50 μm, typical of hydrated silica where the

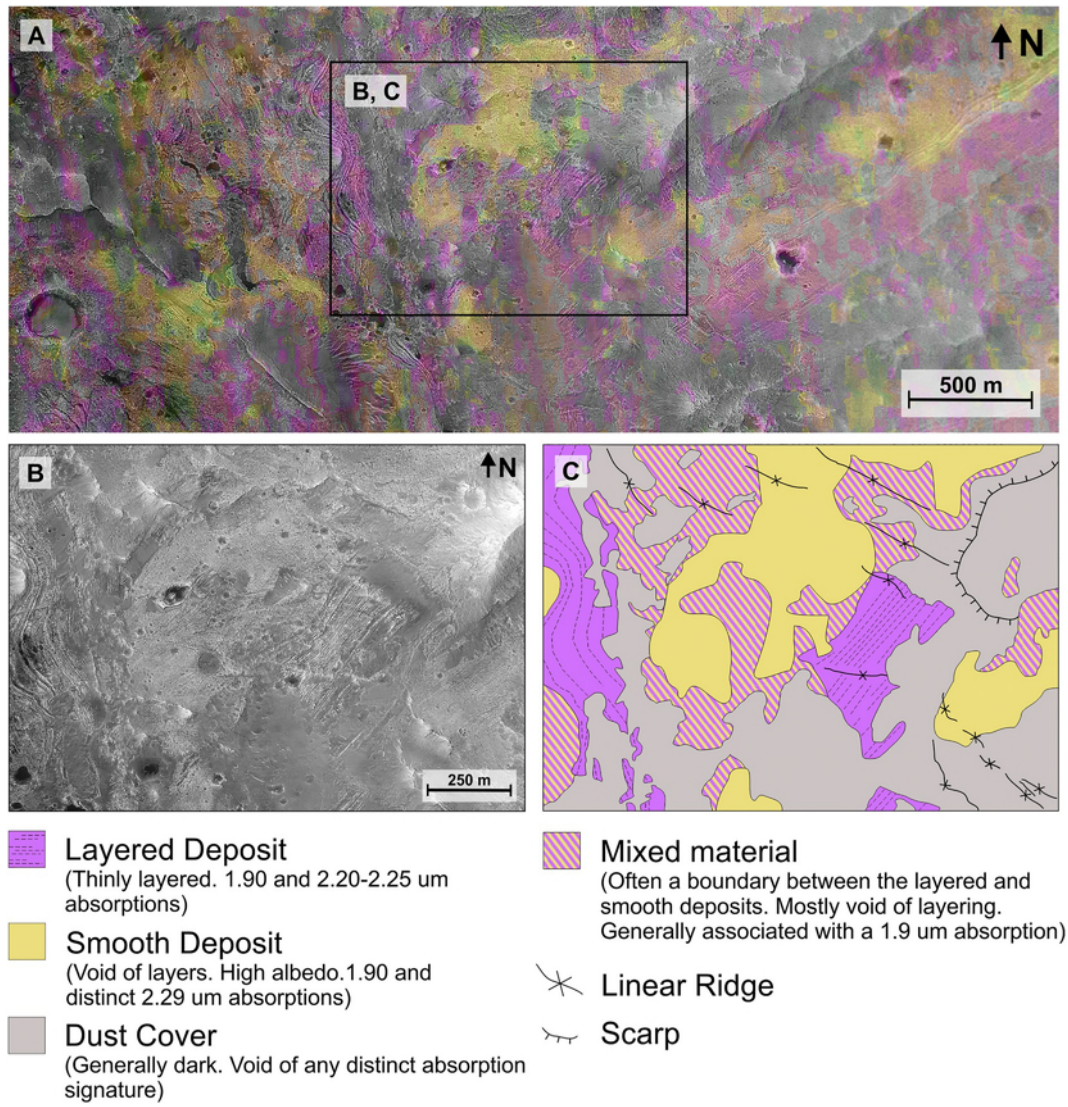

Figure 3. Geological mapping of sample area of the lower equatorial layered deposit based on absorption highlights of Compact Reconnaissance Imaging Spectrometer for Mars (CRISM) summary parameters (R = BD1900_2, G = BD2290, B = SINDEX2). (a) A CRISM RGB composite filtered to display yellow (absorptions at 1.90 and 2.29, Mg/Fe phyllosilicate) and magenta (absorptions at 1.90 μm and broadly 2.10–2.40 μm). The CRISM RGB composite is semi-transparent over HiRISE image ESP_025637_2020. (b) Sample area of ESP_025637_2020 for visual reference with the adjacent geologic map. (c) Geological map of small area to demonstrate the two morphologies with the two identified spectral types from Figure 2b.

1.4 μm band is shifted to longer wavelengths as crystallinity increases (e.g., from 1.38 to 1.42 μm) (Viviano-Beck et al., 2014). The absorptions in the 2.20–2.25 μm range are indicative of a metal cation of Al or hydrated silica (Clark, King, et al., 1990; Clark, Swayze, et al., 1990; Ehlmann et al., 2009; Flahaut et al., 2015). The second signature type has a strong absorption at 1.9 μm, a unique absorption at 2.29 μm, and a distinct spectral slope in the 2.3–2.32 μm (Figure 2c, spectra 4, 5, and 6 in right column). There is also faint evidence of a weak absorption at 1.4 μm. A 2.29 μm absorption implies a metal cation of Mg or Fe-OH (Bishop et al., 2008; Viviano-Beck et al., 2014), and is easily distinguishable from Al which is diagnostic at 2.20 μm (Flahaut et al., 2015).

These two signature types are associated with specific geomorphologies. Spectra 1–3 (Figure 2c left column) are predominately associated with layering, whereas spectra 4–6 (Figure 2c right column) are always associated with a smooth, high albedo deposit, which is void of layering (Figure 3). The smooth deposit lies stratigraphically above the layered sections and often appears to overlap it. Layered sections often contain raised non-layered linear

ridges that exhibit high albedo (examples of non-layered linear ridges found in the accompanying Supporting Information S1).

A total of 98 layers were measured in the Lower ELD showing a layer thickness range of 0.12–8.34 m and an average layer thickness of 1.50 m (Figure 4a). No sequences or trends were apparent except that average layer thickness increases with elevation (Figure 4a). Layer attitudes in the Lower ELD were difficult to measure due to many layers being less than a meter thick. It was at times difficult to discern if layers are near vertical or if they are so thin that they give the illusion of being vertical. With instances of steeply dipping layers, accompanied with the non-layered smooth material which separates layered sections, the Lower ELD gives the impression of entire separated "blocks" that have been tilted to a vertical orientation (Figure 4c). In any case, the maximum dip measured within the Lower ELD with reliability was 29° (Figure 4d). Furthermore, the majority of dips measured within the Lower ELD were <8° (e.g., Figure 4e). It is still possible that some layers exist within the Lower ELD that could be dipping >29° or even close to vertical, because some sections of layering are so thin that a reliable dip plane is difficult to determine.

Layering within the Lower ELD is characterized by non-horizontally continuous sequences that are truncated by non-layered, smooth material (Figure 4c). These truncated sections of layering have an angular appearance and their assembling appears chaotic (Figure 4c), implying they may be bounded, dislocated, and tilted by faults, or emplaced after a mass-wasting event. There are several small knobs superimposed on layering as well (Figure 1d). As described in Figure 3, the smooth non-layered deposit appears to cover layering.

4.2. ELD Mound

The ELD Mound is the predominant feature of Becquerel. The deposit has a particularly high albedo in contrast to the crater's interior and the surrounding plateau. Its irregular shape covers a surface area of approximately 1,000 km^2 and is nearly 800 m high relative to the surrounding crater floor. The north side has a very gentle 1.5–4.5° slope, whereas the south side is slightly steeper at 5.0–7.5°. It has a total volume of approximately 393 km^3 worth of material. It is characterized by the presence of a hydrated spectral signature, thinning and thickening sequences, areas of heavy deformation, and major faulting.

Spectral analysis using four CRISM observations identified that the ELD is dominated by one signature type (Figure 5). We present three example signatures from various areas of the mound which show a broad absorption in the 1.9–2.1 μm range, a 2.4 μm absorption, and a broad absorption in the 1.4–1.6 μm range. This 1.4–1.6 μm absorption is more focused at 1.4 μm in signature 7, whereas it is more focused at 1.5 μm in signatures 8 and 9 (Figure 5d). No signs of mineralogical transitions were identified within the mound apart from the large difference between the crater floor and the mound itself.

A total of 173 layers were measured within the ELD Mound averaging 3.8 m (±0.4 m) with a range of 0.37–8.44 m (Figure 6). Layer thickness measurements performed previously in Becquerel by Cadieux and Kah (2015) produced an average of 3.6 m and compares nicely with our measurements. Several thickening and thinning sequences are apparent and have been refined by averaging the layer thickness values every 50 m and advancing the averaging in 10 m intervals upsection (vertical green trendline Figure 6a). However, when the section is taken as a whole, layer thicknesses remain more or less constant upwards in section with only a slight 1 m decrease in average thickness. Interestingly, both the Lower ELD and the ELD Mound share a common maximum layer thickness (8.34 and 8.44 m respectively).

Layering varies in appearance across the ELD Mound and is more complicated than layering in the Lower ELD. Bedding and erosional attributes are shared among layers spanning all elevations of the mound, as well as internal layering observed from large sections exposed from downward erosion. However, the southern side of the mound has a predominance of N-S trending yardangs compared to the northern side. The northeastern area of the mound is characterized by alternating lenticular bodies henceforth referred to as the tinted facies (T) and pale facies (P) (Figure 7). Facies T is characterized by sigmoidal structures that tend to pinch out, have chaotic layering, low albedo in respect to the rest of the mound, and a slightly different erosional pattern from the surrounding pale facies. In some cases, it is possible to observe an erosional base at the contact between them (Figure 7). The orientation and the shape of the lenticular bodies remain mostly parallel to each other throughout the northeastern area and retain a NW-SE trend.

On the western side of the ELD Mound the tinted and pale facies take on a different appearance (Figure 8). Bedding is cut by two sets of surface changes, or discontinuities, oriented predominately E-W and partially

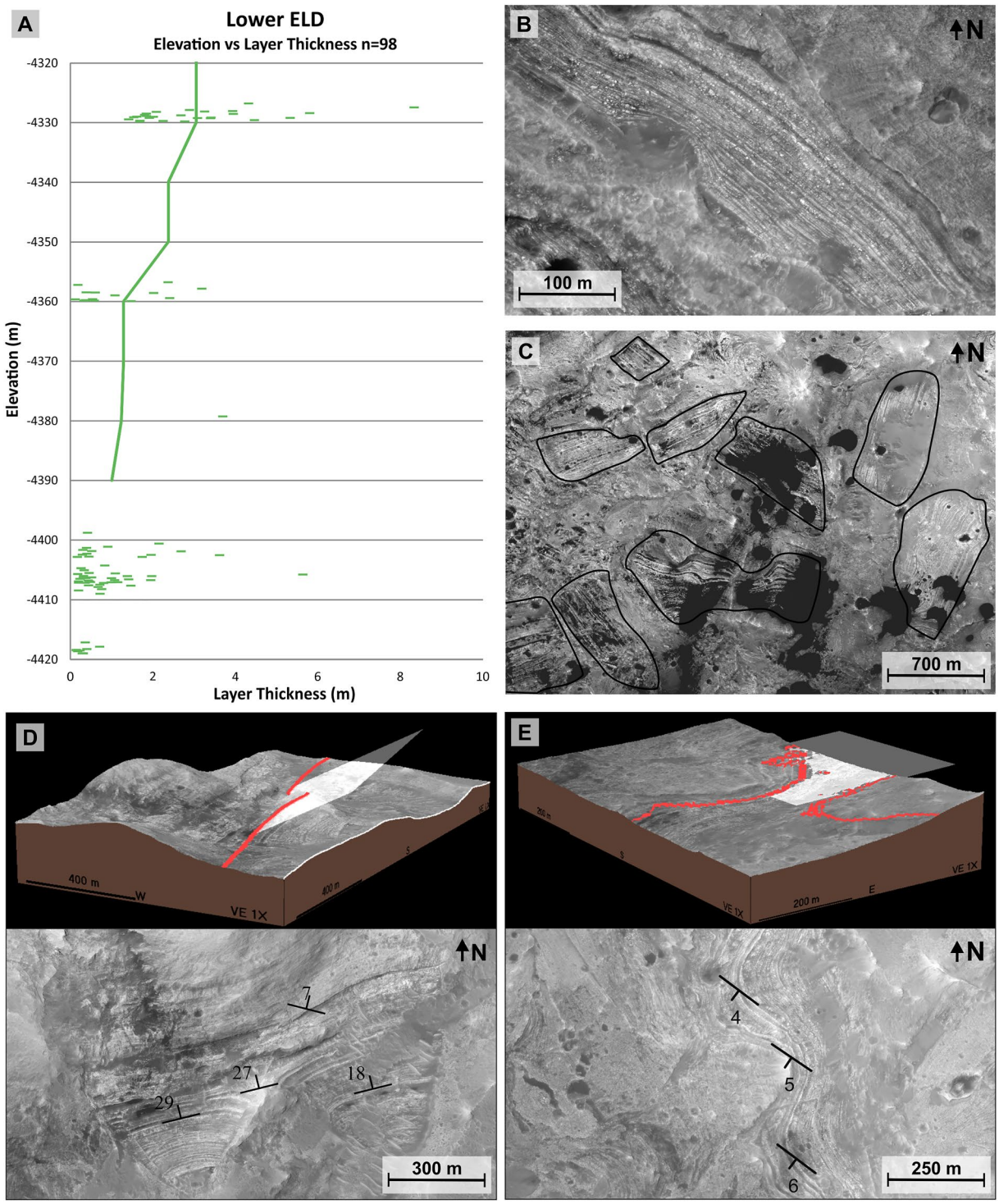

Figure 4. Layer measuring within the Lower equatorial layered deposit (ELD). (a) Lower ELD layer thickness measurements. Layer thickness are shown as short horizontal green lines to represent layering. The vertical green trendline is the values created from averaging the layer thickness values every 50 m and advancing the averaging in 10 m intervals upsection. (b) Example of the thin Lower ELD layers. HiRISE image ESP_025637_2020. (c) Several truncated sections of layering are outlined in black (d) Example of the highest measured dips in the Lower ELD in both 3D and top down views with dip measurements. In top down view one can have the impression of vertical layering. The 3D scene is taken from the Orion software and shows the attitude of the steeper layering. The transparent plane represents the best-fit plane to layer outcrop (traced in red). In this case the plane has a calculated dip of 27° derived from Orion. The red line traces the limit of a layer, which is the line of intersection between a geological horizon and the topographic surface. HiRISE image ESP_025637_2020. (e) Example of the typical lower inclined dips in the Lower ELD. The 3D scene is taken from the Orion software and shows a transparent plane of 5°. Symbology of the 3D scene is equal to Figure 4d.

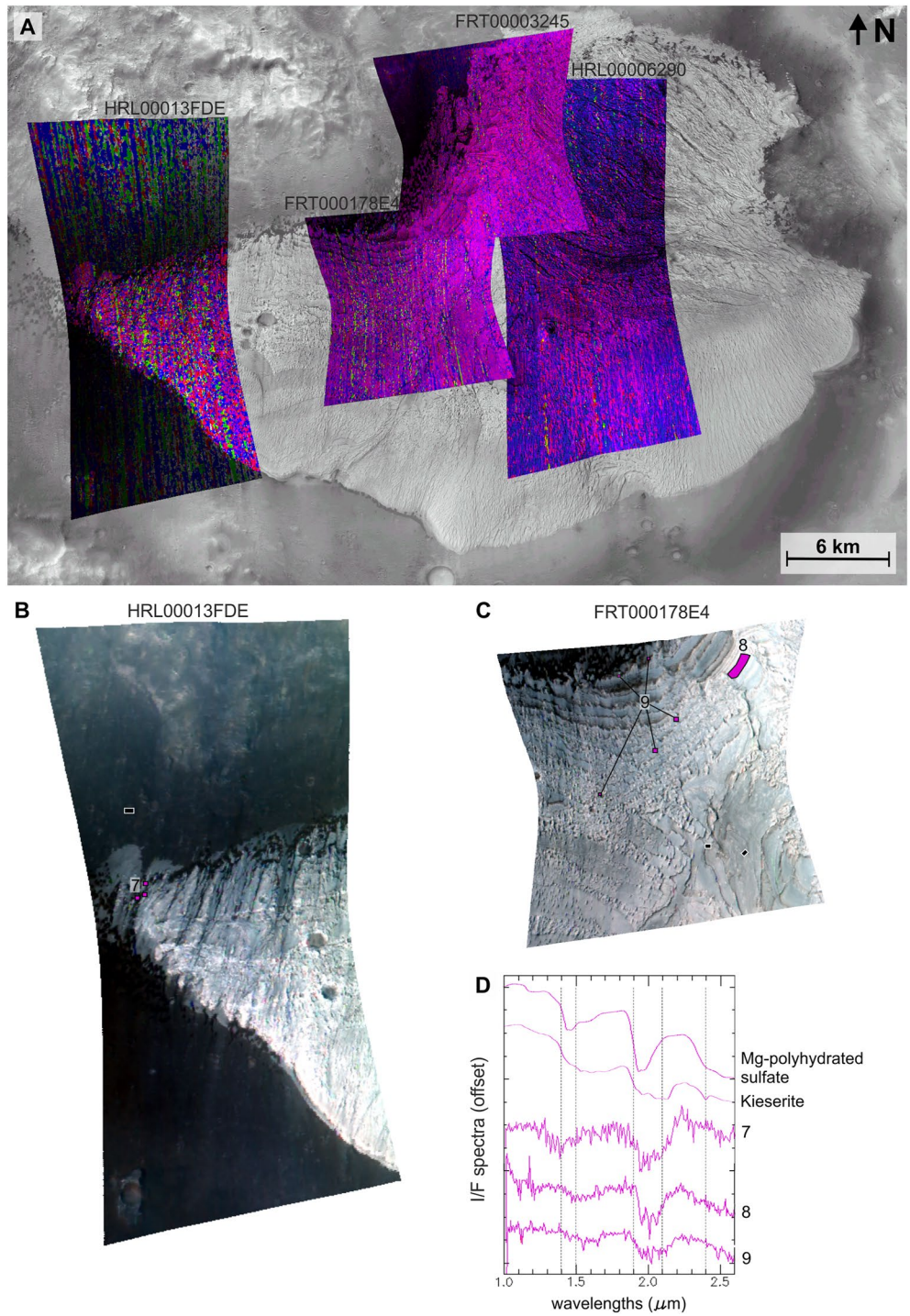

Figure 5. Compact Reconnaissance Imaging Spectrometer for Mars (CRISM) Analysis of the equatorial layered deposit (ELD) Mound. (a) CRISM RGB composites of observations FRT00003245, FRT000178E4, HRL00013FDE, and HRL00006290 projected over a CTX mosaic. Summary parameters highlighting hydrated mineral detections (R = BD1900_2 [0.0–0.032], G = BD2290 [0.0–0.011], B = SINDEX2 [0.0–0.023]). (b) False color composite of HRL00013FDE. The ROI location of spectral signature "7" is indicated by the three magenta squares. The black square indicates the location used as a common denominator to produce the presented ratio. (c) False color composite of FRT000178E4. The ROI locations of spectral signatures "8" and "9" are indicated by the magenta polygons. The black squares indicate the location used as a common denominator for ratios. (d) Three separate ratioed spectra identified in HRL00013FDE and FRT000178E4. Library spectra; kieserite F1CC15 and Mg-polyhydrated sulfate CJB366.

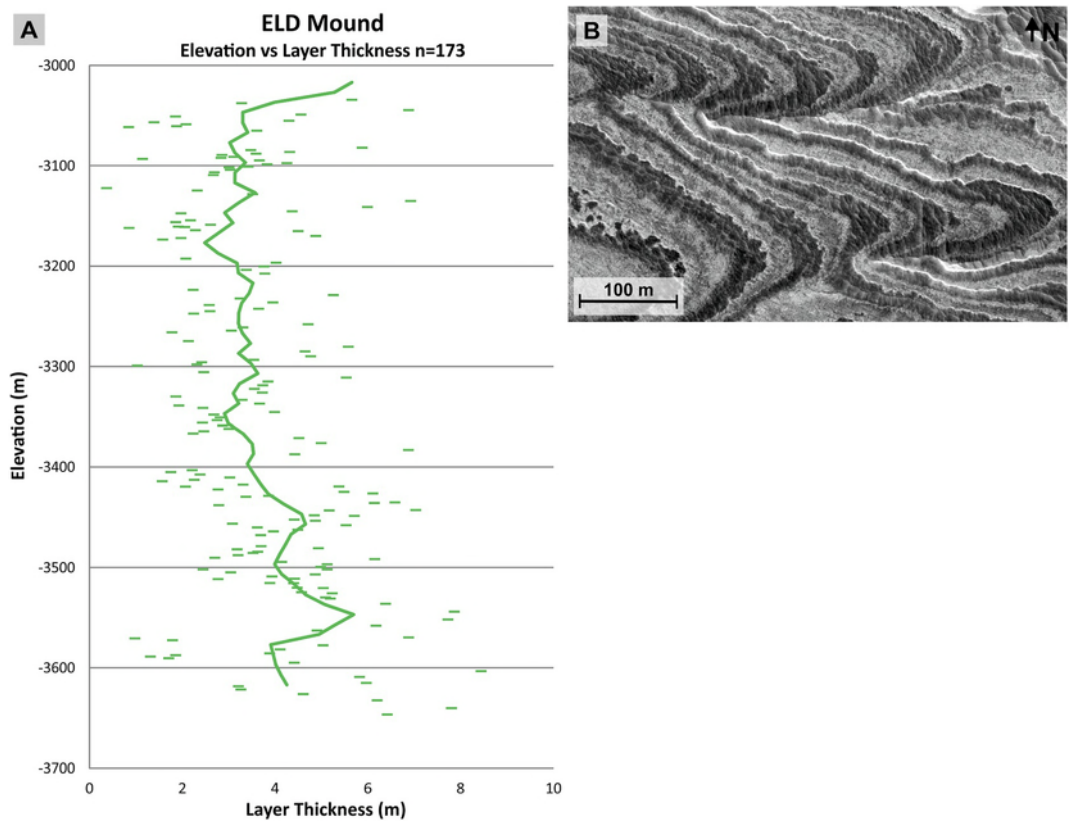

Figure 6. (a) Equatorial layered deposit (ELD) Mound layer thickness measurements. Layer thickness are shown as short horizontal green lines to represent layering. The vertical green trendline is the values created from averaging the layer thickness values every 50 m and advancing the averaging in 10 m intervals upsection. (b) Example of ELD Mound layers. HiRISE image PSP_004078_2015.

NE-SW (Figure 8a). The E-W set is characterized by light-toned and smooth surfaces that form long discontinuities (≤10 km). They have eroded differently than surrounding material which has higher albedo and a greater yardang prominence. The NE-SW trending discontinuities are shorter (1–1.5 km), often terminate at the E-W discontinuities, and are collinear with yardangs. In both of the trends, no significant displacements were observed. Further southeast, the E-W trend aligns well with contacts between the tinted and pale facies. They are cut by a unique N-S linear scarp which curves west upwards in elevation (Figure 8b).

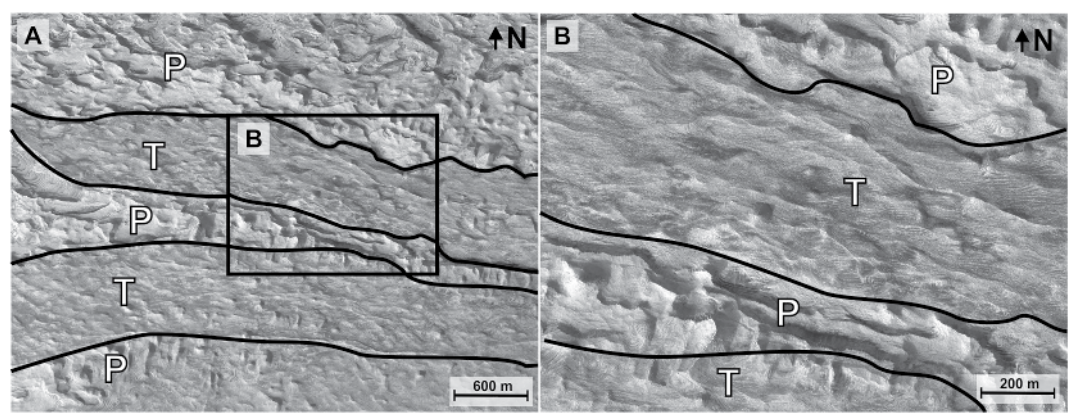

Figure 7. (a) Contact between the lenticular bodies belonging to the tinted facies (T) and the planar beds belonging to the pale facies (P). (b) Zoomed in area of the tinted facies (T). HiRISE image PSP_003656_2015.

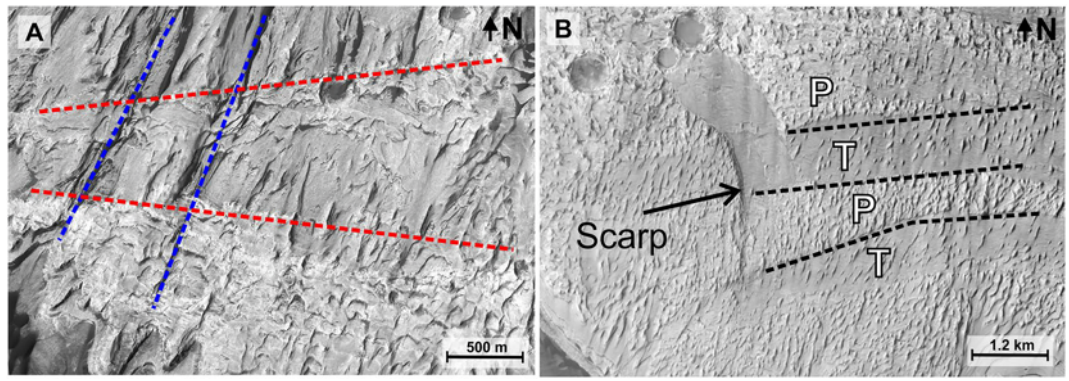

Figure 8. Two main trends of discontinuities mark changes in physical appearance of areas in the western side of the equatorial layered deposit Mound. (a) E-W traced by red dashed lines and NE-SW traced by blue dashed lines. Across the E-W discontinuities the material seems to be different from the surrounding, showing light-toned and less eroded surfaces. HiRISE image ESP_016077_2015. (b) CTX image P01_001546_2016 showing the same E-W trend that aligns with contacts between the tinted and pale facies. This trend is cut by a N-S to NW-SE scarp.

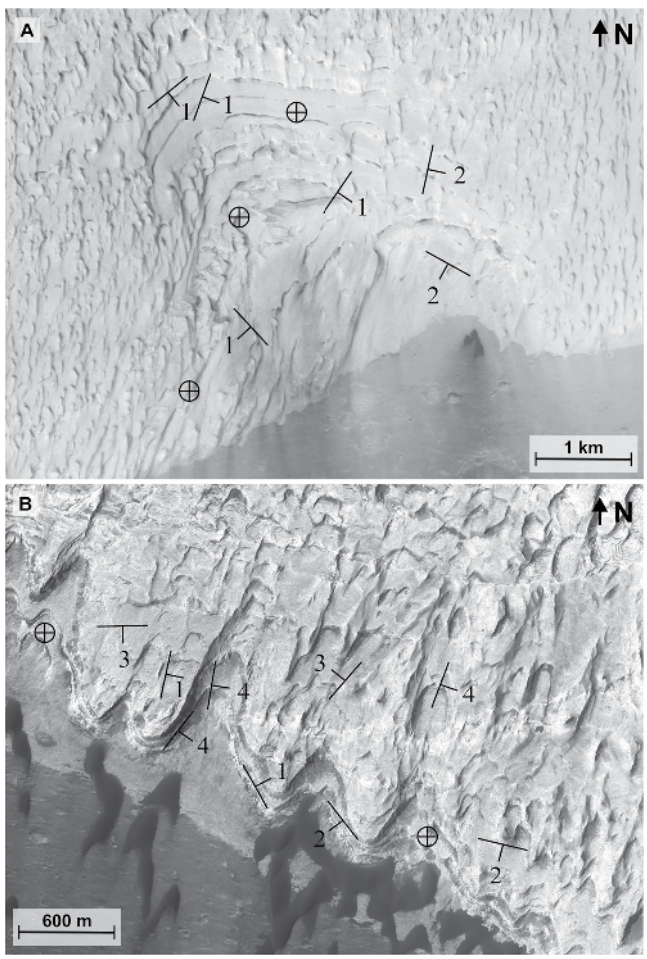

Figure 9. Horizontal and sub-horizontal layering observed in the south side of the equatorial layered deposit Mound near the crater floor. (a) South central side. CTX image G19_025637_2021. (b) Southwest side. HiRISE image ESP_034419_2015.

Layer attitudes measured in the ELD Mound range from horizontal to 44° (Figures 9–11). Layers on the north, west, and south sides of the mound are all horizontal where they meet the crater floor (Figures 9 and 10) and tend to remain horizontal upwards in section. Layer attitudes >4° are always associated with nearby faulting, and areas with the highest dips appear to be resting upon horizontal layering (e.g., Figure 10). These instances give the impression of progradation, fault transport, or even a massive landslide where entire sections of layering have been transported from higher elevations by ≤1 km and reoriented. Another example of layers diverging from horizontal is observed in the south where layer attitudes appear to be influenced by a fault expressed as a NE-SW oriented ridge (Figure 11). These layers follow the ridge for nearly 2 km while keeping a 12–15° westerly dip, but return to near horizontal as they diverge from the ridge (Figure 11).

The ELD Mound contains several fault sets exhibiting meters of horizontal offset (Figures 12 and 13). There are major faults which horizontally offset layering, and at times the tinted and pale facies by more than a kilometer (Figure 12e). Between these major faults are branching minor faults (e.g., Figure 12). In Figure 12c two major faults with the same orientation form a graben structure with a 40° slope angle. The NW-SE faults show a displacement likely produced from an extensional component of the strain and also the high dip angle of the faults is appreciable. The apparent horizontal displacement (or strike separation) of 40 m suggests at least a small strike-slip component, however it could also be produced by pure extensional faults later affected by erosion or by the interference between layering attitude and fault slip vector. Some faults have been infilled with a high albedo material and are raised 1–2 m (Figure 12d).

At the top of the ELD Mound resides a 200 m deep depression that is 8 km in diameter (Figure 13a). The depression is circular and contains a raised knob 150 m in height. This area is characterized by radial faults, originating from the depressed center (Figure 13). Many of these faults have also been infilled producing ridges (Figure 13b).

4.3. Fan Shaped Landforms

Faint evidence of eroded channels is observed on the north side of the interior crater (Figure 14a) where two channels incise almost 500 m and debouch

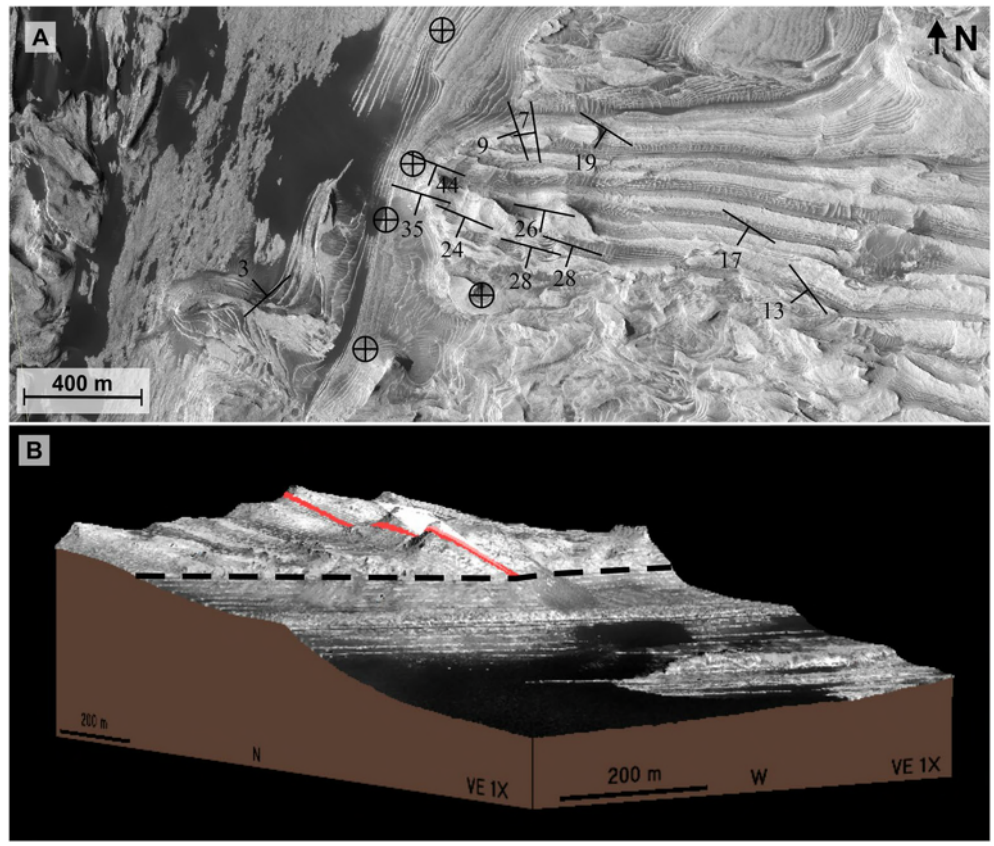

Figure 10. Highly inclined layers observed at a higher elevation than horizontal layers at the bottom of the equatorial layered deposit (ELD) Mound near the crater floor. (a) The north central side of the ELD Mound and the crater floor with strike and dip measurements. (b) 3D view with red out lining a layer dipping south 35°. Black dashed line marks the contact between the inclined and horizontal layers. HiRISE image PSP_001955_2015.

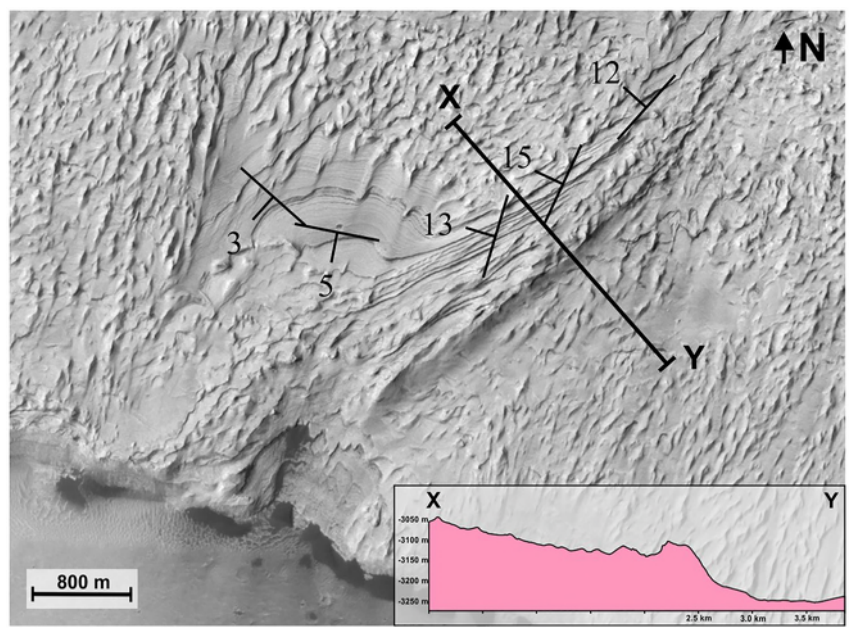

Figure 11. The beds change attitude in correspondence of the NE-SW ridge. As shown by the topographic profile, this ridge produces 100 m of relief. CTX image P01_001546_2016.

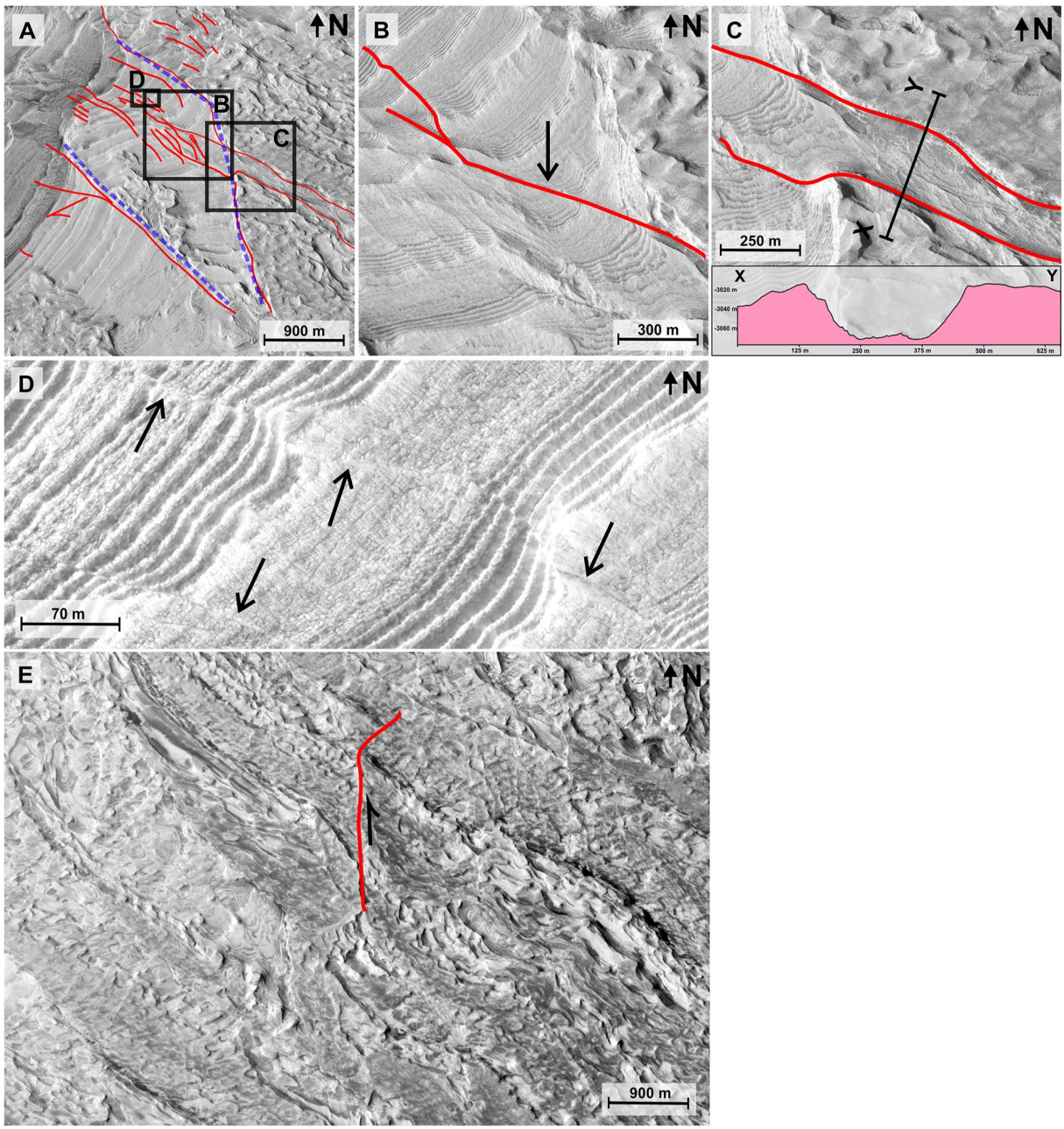

Figure 12. Example of faults observed within the north central area of the equatorial layered deposit Mound. HiRISE image PSP_001955_2015. (a) The main faults in the northern sector are indicated with red lines. A triangular block is marked by a blue dashed line. (b) The displacement of the layered material by the NW-SE faults is pointed by the black arrow. (c) NW-SE oriented graben and topographic profile. (d) Examples of faults perpendicular to layering that have been infilled with a light toned material (indicated by black arrows). (e) Example of a fault that separates a section of the P-T facies by more than a kilometer.

in the crater floor forming two fan shaped bodies (Figure 14b). They do not extend to the higher terrain of the Becquerel crater rim and are associated only with the interior crater.

The channels are partly buried, but one of them shows a sinuous shape, a U-shaped cross section, and amphitheater-shaped alcoves. These morphological characteristics suggest the importance of sapping processes in its formation and/or evolution (Figures 14b and 14c). The fan-shaped landforms show a stepped geometry with low-dipping and high-dipping surfaces which suggest a formation as a delta (or fan delta) in overall transgressive conditions (de Villiers et al., 2013). Still, an exhumed channel is present, suggesting at least a phase of water level drop (Figure 14b). According to the slope breaks in the deltas, water level appears to have fluctuated between

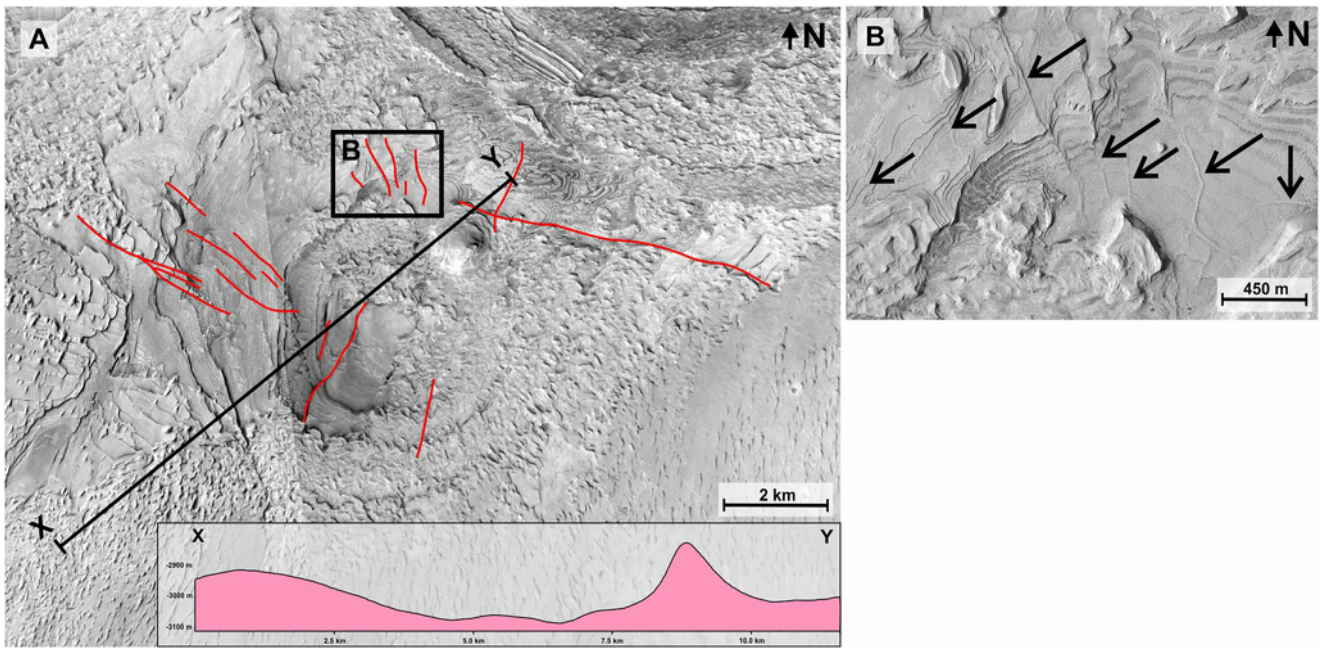

Figure 13. Circular depression on the top of the outcrop. (a) Radial faults affecting the top sector (traced in red). Cross-section A-A′ shows the vertical relief of the depression and the small circular knob. CTX images G19_025637_2021 and P12_005845_2021. (b) Black arrows point out the ridges occurring along several faults. HiRISE image PSP_001955_2015.

−4,100 and −4,300 m below MOLA datum (Figure 14c). These values are consistent with the ones identified by Salese et al. (2019). Locally, shoreline remnants might have been preserved from erosion (Figure 14a). Although the area lacks HiRISE coverage, a total of 14 layers in the east landform and 8 in the west landform are resolvable in CTX images. Where possible, dips of the exposed layering were measured and found to increase upwards in elevation (Figure 14d). From −4,230 to −4,045 m elevation, dips increased 0–12°. Further down from the deltas, flat-lying deposits might correspond to prodelta or basinal materials, but these sedimentary units are covered.

5. Discussion

Spectral analysis, layer measurements, and structural analysis show a complicated geological history within Becquerel. The approximately 700 m elevation difference between the Lower ELD and the ELD Mound is interpreted to have had a substantial effect on the alteration of these deposits. The separation of these two ELDs from each other offers a rare opportunity to observe the effects that elevation has on their composition and the effects of water level and fluid expulsion intensity during their evolution. Possible depositional methods are presented, as well as a prepared sequence of events. Here we describe the discrepancies within both airfall and fluid expulsion scenarios, and then provide a framework for visualizing what hydrogeological activity could have looked like based on our observations. The observations carried out in this work highlight the advantage of combining a variety of data sets to fully appreciate the changing environment present in many of these craters in Arabia Terra.

5.1. ELD Fault Formation

Observations show that the structural setting in both deposits is quite complex. Within the ELD Mound, faults were identified from observed displacement of layering and also inferred from linear structures that cross-cut layering or changes in layer attitude. Both normal and strike-slip components were identified indicating that the ELD Mound could have been in a state of transtension at some point during its history. The triangular block occurring in the northern sector (Figure 12) is interpreted to be bounded by normal faults. Although vertical displacement is not visible, the abundance of minor faults within the block that disrupt layering, combined with steeper, more variable layer attitudes, demonstrates that the block has shifted in relation to its surroundings. The adjacent block shows only a few minor faults with very little displacement and no change in layer attitudes. A

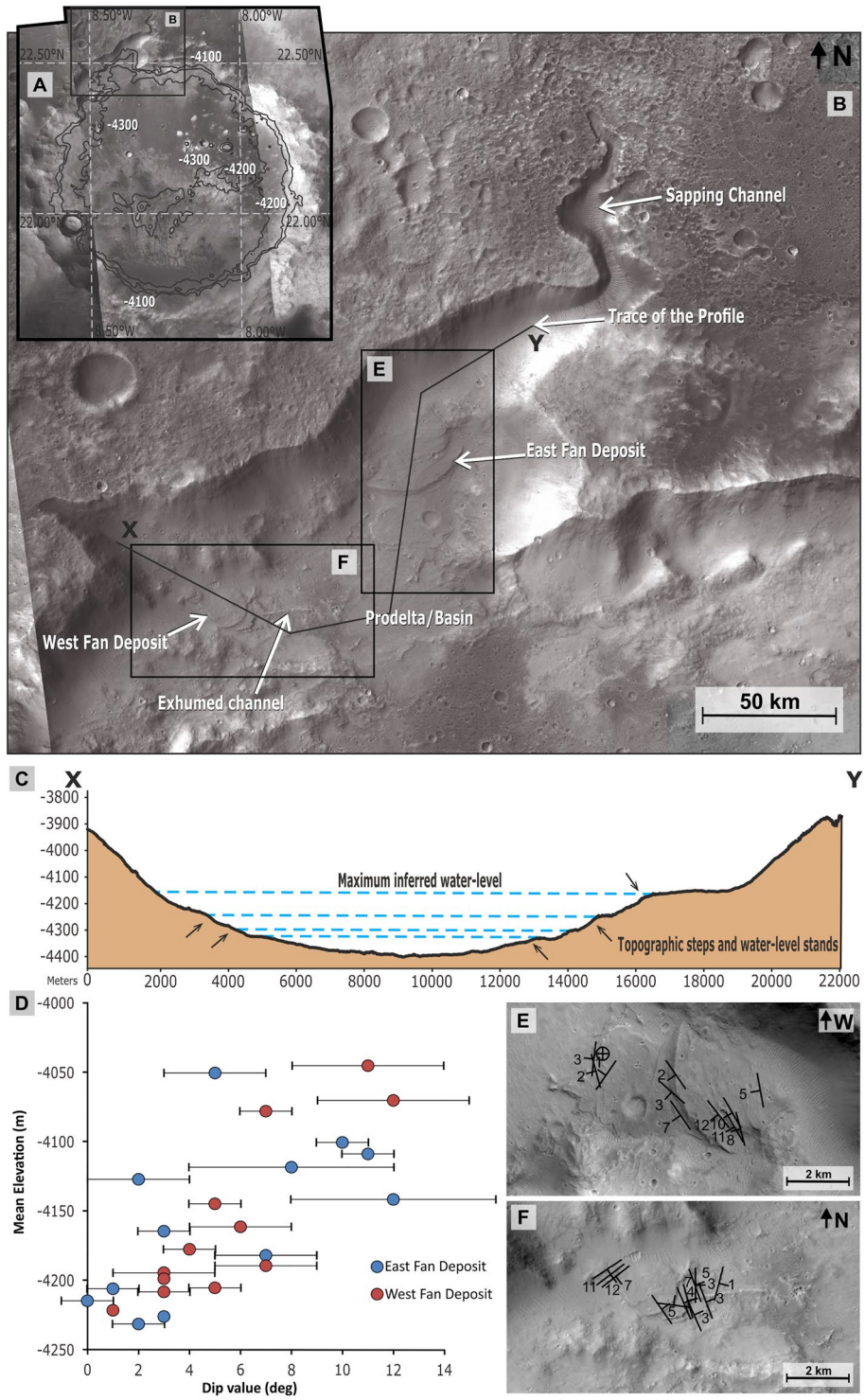

Figure 14. Two fan shaped deposits observed in the interior crater at the northern rim and accompanying sapping channel. (a) Overview of the interior crater with contour lines showing the important elevations values of −4,100, −4,200, and −4,300. (b) Close-up of the fan shaped deposits and all the associated features labeled. CTX image G19_025637_2021. (c) Cross section *X*–*Y* shows the shared benches (or topographic steps) in the deposits. (d) An elevation versus dip graph of the exposed layering within the fans. Dip measurements derived from CTX derived topography (6.2 m/px). Error bars show the ± dip value error for each measurement. The average dip error is 1.5°. (e) Dip values of the East Fan Deposit. (f) Dip values of the West Fan Deposit.

NW-SE structural trend is also shown, with the two major faults bounding a graben-like structure and minor branching faults within the major ones. At the intersection between these structures there is no evidence concerning the relative chronology. No displacement was found constraining the posteriority of one or the other.

The lack of such evidence makes it difficult to establish if the observed minor faults are older than the inferred block bounding faults. However, the extensional stress component was recognized, together with a possible strike-slip component suggested by the horizontal offset. Nevertheless, despite the inferred transtensional regime, there is no obvious evidence of releasing bends with negative flower structures, but this could be due to a minor stress causing the deformation. For the uncertain structures, the kinematic interpretation is more difficult because of the paucity of evidence. The northern inferred fault bounding the triangular block is oriented NNE-SSW (Figure 12). The same orientation is present in the southern area, where a NNE-SSW fault reoriented the hanging wall layers from near horizontal to a 15°W dip (Figure 11). The positive relief of this structure suggests a strong resistance to erosion in respect to the surrounding material. This may be due to cementation induced by mineralized fluids which used the fault deformation zone as preferential pathway. The steeper layers on the hanging wall may also be an indication of extensional kinematics. Thus, if this structure is correlated with the inferred northern fault, the most plausible hypothesis for the formation of the triangular block is within an extensional regime. The intersection between the NNE-SSW ridge and the E-W discontinuities in the southern sector (Figure 8a) does not reveal the relative chronology as well as for the structures in the northern sector. Furthermore, it is unclear if E-W structures (Figure 8a) are faults. In fact, these discontinuities interrupt the down-dip bedding, but no evident displacement has been found.

It is difficult to determine if these E-W structures (Figure 8a) are related to the tinted and pale facies (Figures 7 and 8b). Although they are similar in spacing and orientation, the E-W structures might be separate features that bound the tinted and pale facies, exploiting the weaknesses of the bedding surfaces. The E-W structures might be described as transgressive contacts with a pre-existing cliff topography, where these portions of the mound could be interpreted as the result of cataclastic processes (e.g., fault gauges or local landslides). Another possibility may be that a widespread migration of mineralizing fluids along the E-W faults/fractures took place and cemented the deposits, allowing different responses to erosion.

In the northern sector a few cataclastic processes were assumed. The cases proposed in Figures 12a and 12b are conceivable as fault gauge or fault breccia, since the evidence is based less on their appearance and more on their occurrence along certain faults, as well as their scale and abundance in the northern sector. The high variability in the orientation of the structural features culminates in the top sector, where the faults radiate outwards from the circular depression (Figure 13a). The faults in the top sector present ridges that likely formed from cementation after cataclastic processes and/or deposition of material from fluid circulation within the fault zones. The entire northern area is affected by intense fracturing following two trends perpendicular to each other: 130° (almost parallel to the extensional faults) and 40°. The spatial pattern resembles that of so-called *neotectonic joints* (i.e., systematic or non-systematic joints) on the Earth (Hodgson, 1961; Price & Cosgrove, 1990), but in this case there is no reference to the fracturing chronology.

The northeastern side of the ELD Mound has many instances of intact sections of layering being brought from higher elevations and reoriented, often positioned in high angles (Figure 10). This could be the result of some mass wasting event such as a landslide or gradual creep. Although landslides are controlled by a number of factors (Hungr et al., 2014; Varnes, 1978), since the northern slope of the ELD Mound is $\leq$4.5°, it is unlikely that gravity alone could be the sole driver of the observed movement of these intact sections because a significant force is needed to overcome the internal friction. On Earth, the contribution of gravity in a landslide is a main force, however landslides usually have multiple causes and the majority of them require some kind of slip surface (Skempton & Petley, 1967). On Mars, gravity is also less than half of Earth's, and thus it is more difficult to overcome internal friction by the force of gravity alone. Thus, we propose that conditions and processes taking place in the interior of the mound such as lubrication from water or salts, and/or internal pressure from expansion induced by salt formation (Dronkert & Remmelts, 1996) are needed. While salt diapirism is not a depositional method that explains the observed layering, it can be used as a way to explain the existence of these movements. Further, salts in the interior of the ELD Mound could have dissolved, leading to the formation of the central depression, and this loss of volume contributed to the massive detachment and movement of material downslope. Alternatively, a submerged ELD Mound is also a viable setting for producing a landslide event. On Earth, the slope gradient of submarine landslides is very gentle, on average 4° (Ye, 2017). This is largely due to increased

pore pressure and decreased frictional resistance of the submerged material (Masson et al., 2006). Thus, despite the gentle slopes of the ELD Mound, in a submerged setting a landslide is more probable.

The complex structural pattern throughout the main ELD mound is likely the result of compaction and internal collapse within the deposit. Internal collapse could have been exacerbated from water saturation, dissolving of internal salts, or even marsquakes. The relatively flat crater floor surrounding the mound and the unaffected rim of the interior crater both indicate that if collapse of the crater floor was a contributing factor, then collapse is isolated and located directly underneath the mound. Weakness in the crater floor directly underneath the mound could have been influenced by void space and conduits that groundwater utilized during fluid expulsion. An analogous feature was documented by Sunwall et al. (1983) who analyzed seismic data of the faults above a salt dome in the Gulf of Mexico. They recognized numerous radial faults emanating from the salt dome and concluded those faults were produced as a result of the diaper rising. Despite the difficulties in constraining the occurrence of a salt dome beneath the mound in Becquerel, the mechanism of internal collapse could still be discussed, perhaps due to mud diapirism or in any case to the rise of a material less dense than the surrounding. However, diapirism can produce a contemporary summit crater (circular depression) related to the extension, and peripheral landsliding by the increase in slope. Considering the hydrated sulfate compositions determined from this study, salt expansion as a trigger for landslides as demonstrated by Bishop et al. (2021) could have contributed to mound deformation. In the scenario that deformation occurred during spring activity, faults and landslides could have been lubricated by highly mineralized waters. Alternatively, they could have been lubricated by unobserved internal salt rich layers.

5.2. Deposition of ELDs

5.2.1. ELD Mound

The formation of layered mounds on Mars has been an on-going and difficult geologic process to resolve, however there are several particularities that the ELD Mound in Becquerel exhibits, that when taken in reference to other features in the crater (i.e., the Lower ELD and the fan shaped landforms) can significantly advance our understanding. These include thinning and thickening layer thickness sequences of horizontally continuous layers, large-scale deformation features, and mound shape. Possible depositional methods of the ELD Mound can be loosely categorized as aeolian in a dry crater, aeolian in the presence of water (with water activity ranging from a full on lake to sporadic fluid expulsion), or strictly fluid expulsion. All possibilities must also take into account the added aspect of wind erosion playing a role in the present mound shape.

5.2.1.1. Eroded Crater Infill Versus Forming as a Mound

In order to assess plausible depositional environments, we should first consider whether the ELD Mound once extended over the entire crater floor. There is no ejecta debris covering the main ELD mound nor is there any symmetry of the mound with the interior crater rim, thus suggesting that the interior crater was already formed before deposition of the mound began. In an airfall scenario, deposition may have occurred uniformly throughout the crater, or at least one would expect to find deposit remnants elsewhere in the crater. If the ELD Mound had once filled the entire crater (e.g., Crommelin [Franchi et al., 2014], Firsoff [Pondrelli et al., 2015], or Henry [Day & Catling, 2020]), roughly 37,000 km^3 of material would have been removed, plus another 1,800 km^3 for the interior crater. The ELD Mound also only contains yardangs on the southern side, implying aeolian erosion has not been very active on the northern side. Continuous eddy, as simulated by Day et al. (2016), can erode infilled craters into central mounds. However, this scenario is problematic in Becquerel due to the duality of Lower ELD and the ELD Mound. Since the ELD Mound post-dates the interior crater, if Becquerel was completely filled, the interior crater would have been filled as well. Yet, the interior crater contains a much smaller deposit, which is counter-intuitive to the ELD Mound having been shaped primarily by wind, as the interior crater would have provided more protection, and thus the Lower ELD should be much larger than it is compared to the ELD Mound. Furthermore, a scenario where one crater undergoes the removal of tens of thousands of cubic kilometers worth of material, while simultaneously a nearby crater remains with an ELD which extends the height of the crater walls (e.g., Crommellin) is unsatisfactory. The sheer volume needed to be eroded in this case leads to a number of problems particularly when coupled with the numerous structural features still present (i.e., not eroded away by wind) (Figure 15). Becquerel crater has been mapped previously and remnant ELDs were not identified in other areas of the crater apart from the Lower ELD and ELD Mound (Ehrlich & Gross, 2020). Ultimately, until further HiRISE images are obtained in other areas of Becquerel, we cannot decisively determine if the Lower ELD and

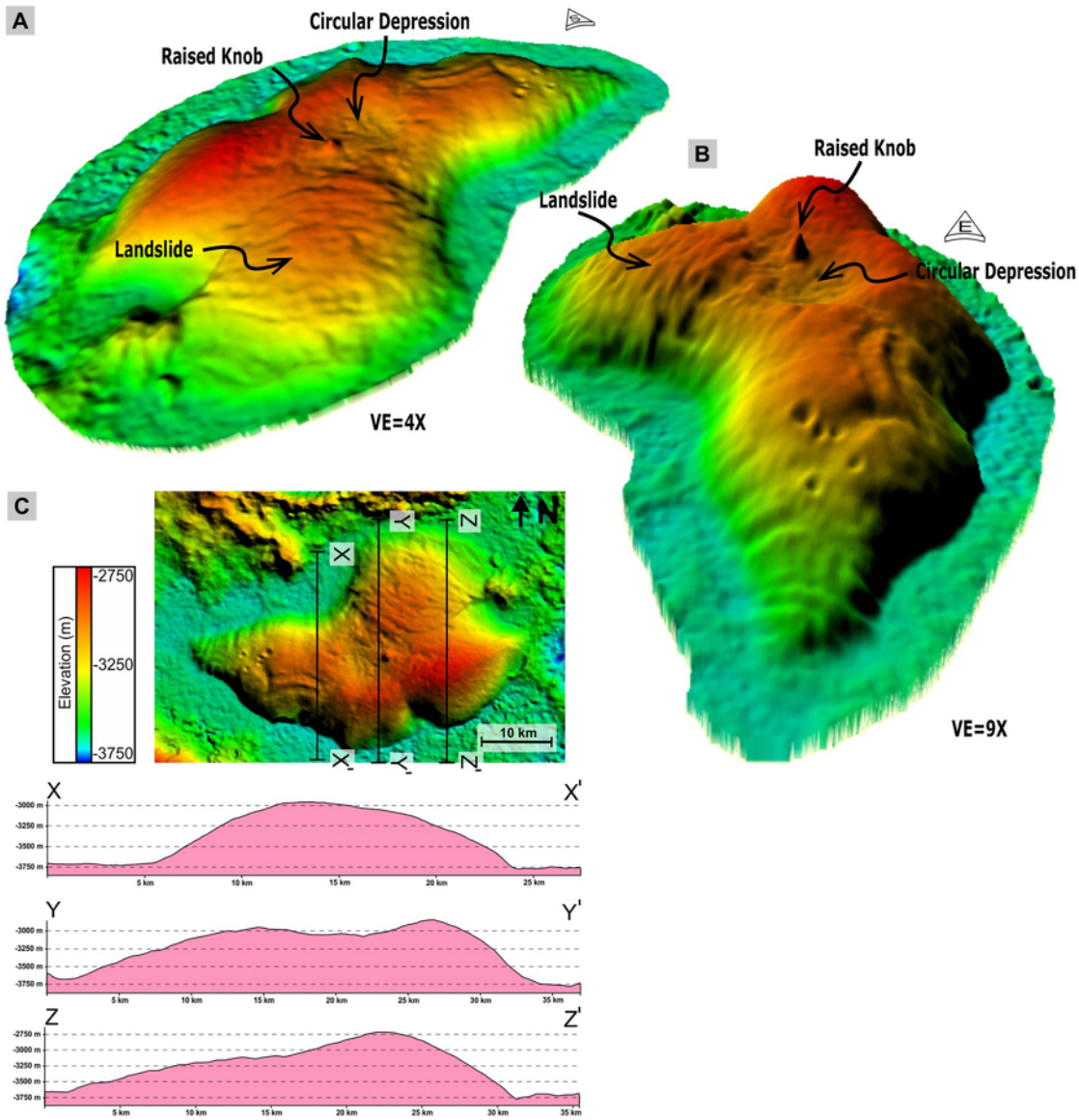

Figure 15. 3D views of the equatorial layered deposit Mound in High Resolution Stereo Camera topography. (a and b) Features such as the landslide, raised knob, and circular depression are dominant topographical features. (c) Cross-sections show the affect that the landslide has had on the northwest side of the mound, whereas the east side does not conform to significant north-south wind erosion linked to Arabia Terra wind streaks.

the ELD Mound are the only instances of layering. It is at times difficult to observe traces of layering in CTX images, and one would expect some degree of ambiguity (e.g., areas of high albedo like the ELD Mound, areas of some strange material juxtaposed against obvious crater material/wall/floor), which are not apparent features in the rest of the crater. Some small areas of the crater floor have irregular and patchy erosion, however both the Lower ELD and ELD Mound are quite obvious in CTX images and HiRISE is only needed for the resolution of very thin layering.

Wind processes as a major influence on layered mounds has been explored previously (Day et al., 2016; Kite et al., 2013). In an effort to explain the paradox of missing material and mound shape, the katabatic winds method of deposition (Kite et al., 2013) can be invoked as a depositional process. However, layering in Becquerel is consistently observed to be horizontal (<4° with no regular dip direction) where the deposit is in contact with the crater floor. This conflicts with the katabatic winds model which requires layered mounds to have outward radial dips. Dips do not radiate outwards like mounds in Valles Marineris and Gale Crater (Fueten et al., 2014; Kite et al., 2013; Schmidt et al., 2018). This implies that all layering was deposited and remained horizontal before

deformation. Wind erosion, while certainly an active process in Arabia Terra, does not appear to be a major influence on the ELD Mound. Although there are north-south yardangs present on the ELD Mound (predominantly on the mound's south side), a north-south wind direction is at odds with the present mound shape (Figure 15). North-south wind streaks on the plateau adjacent to many craters of western Arabia Terra (including Becquerel) have been demonstrated previously to be comprised of mixed material with their connection to eroded ELD material undetermined (Edgett, 2002). Mapping of wind streaks in Arabia Terra has also demonstrated that craters with layered mounds do not always have an adjacent wind streak (Fergason & Christensen, 2008). Furthermore, the duration of this N-S wind direction is not known and considered to be a recent characteristic of Arabia Terra (Dorn & Day, 2020; Fergason & Christensen, 2008). Thus, a vortex/eddy type of wind influence (Day et al., 2016) is more agreeable with our observations. However, in the case such a process was a major erosional contribution in forming the mound's present shape from a large crater infill, then the landslide, raised knob, and central depression (Figure 15) are all very recent geological events as they have not been eroded.

Horizontal bedding is consistent with a lacustrine deposition, however this would again imply extensive and differentiated erosion. According to Andrews-Hanna et al. (2010), the ELDs extended throughout the crater, or at least to the eastern rim, based on the observation of a bench identifiable in the topographic profile crossing both the mound and the eastern rim. However, no remnants of layered deposits were observed elsewhere in the crater (Ehrlich & Gross, 2020).

Thus, we find it is more likely that the current mound represents the general size of the original mound, where only a small reduction to its original extent has occurred. Otherwise, a reason for increased erosion specific to Becquerel would need to be created when there are dozens of craters elsewhere in Arabia Terra (e.g., Henry, Sera, Danielson, Kotido, Crommelin just to name a few) that have retained their crater-wide deposits. Moreover, reworked light-toned material should be visible in the form of dust or dunes.

5.2.1.2. Layering

Layers in a localized mound could have been formed by fluid expulsion, the build-up of sediment within an endorheic basin, or diapirism (Jackson et al., 2011). However, the piling of sediment from drainage into an endorheic basin cannot easily explain the laterally continuous layering of the mound and no evidence of diapiric uplift is observed affecting the rim of the interior crater. Diapirism is not an effective method for layer deposition, however it can explain the observed mound deformation.

There is a plausible relationship between the ELD Mound and the fan shaped landforms (Figure 14) which demonstrates the degree of water activity that occurred in Becquerel. The fan shaped landforms have layering and share three topographical steps (Figure 14c). Layer dips increased with elevation (Figure 14d), which is thought to be indicative of delta geometry (Goudge et al., 2017). These features, accompanied with the morphological aspects, reveals they are likely stepped deltas. However, the increase in dip with elevation might also be influenced by the increasing slope of the crater wall, rather than being solely the expression of an erosional front exposing the interior forset of the deltas (Goudge et al., 2017). Regardless, these features very likely played an important role in the aqueous history within the interior crater. We propose their shared −4,100 m elevation (Figure 14) is strong evidence that a lake might have once existed within Becquerel. Their existence shows that water remained for a time at least in the interior crater, which is bolstered by the same elevation of other deltas and channels in the region (Salese et al., 2019). Interestingly, the −2,700 elevation of the top of the ELD Mound is the exact elevation of the beginning of the Mawrth Vallis channel (Figure 1a; 3D scene available in Supporting Information S1). Thus, if Becquerel had once been filled with water, the water level may have fluctuated between −2,700 m and −4,100 m during the deposition of the ELD Mound and then as the water level receded, Mawrth Vallis formed. Thinning and thickening sequences might reflect a fluctuating water level.

5.2.1.3. Mound Geometry

Features such as the circular depression, landslide, and raised knob (Figures 10, 13, and 15) provide an opportunity to constrain the timing of erosional activities, both past and present, acting on the ELD Mound. For example, if the ELD Mound represents the last vestige of a once crater-wide deposit, then the large landslide (Figure 10) and central depression (Figure 13) occurred relatively recently. However, if the formation of the landslide and central depression was influenced by water activity, then based on current models of past Martian climate (Bibring et al., 2006; Quantin et al., 2010) they would have formed early in the history of the ELD mound due to the cessation of the majority of water activity in the Early Hesperian (Carr & Head, 2010). Thus, if they

are related to water-activity of any kind (whether direct influence from fluid activity or passively in an evaporative environment), then the ELD Mound could not have been much bigger than the present size. Furthermore, the angle of the landslide surface (3–8°) accompanied with Martian gravity make it difficult for a landslide to occur without the aid of other forces (e.g., fluid interaction on the slip-plan and/or doming related to the central depression). If the landslide and central depression are relatively recent events, then proposed erosional processes of the ELD Mound (in both type and duration) must account for their existence, including the small knob on the edge of the central depression (Figures 13 and 15). In a scenario where aeolian erosion is intense and ongoing (Day et al., 2016; Koeppel et al., 2022), the presence of the raised circular knob (i.e., not streamlined or oblique like the observed yardangs) which towers 150 m (Figures 13 and 15) over the top surface of the ELD Mound is not easily explained. The circular depression, the landslide event, and small circular knob are thus more likely to be old events in the mound's history. In this case, aeolian erosion would have been relatively minimal as to allow these structures to persist to the present day. The raised knob might represent a spring mound that was formed from ongoing pressure from below after the landslide event occurred. The landslide might post-date the circular depression since the north rim (adjacent to the landslide) of the circular depression is 150–200 m lower than the average height of the rest of rim. This gives the impression that the north rim of the circular depression was deformed during the landslide event.

5.2.1.4. Tinted and Pale Facies

The tinted and pale facies either represent a compositional or a grain size difference that would reflect differences in the responses to erosion. Although hindered by dust, spectral analysis did not show any compositional differences associated to elevation, layering, or the tinted and pale facies. If the composition is the same, then the variable response to erosion could be explained by detachments along slip surfaces lubricated by salt rich layers and/or water that detached top portions of the ELD Mound (Jackson et al., 2011). The tinted facies is represented by dark lenticular bodies that perhaps represent periods of subaerial non-deposition where the surface was lithified (Pondrelli et al., 2019). Alternatively, the lenticular bodies could represent a contrasting depositional method from the rest of the mound (Day & Catling, 2020), for example, if the mound is being deposited by fluid expulsion which pauses and then dust collects on the mound proceeded again by more fluid expulsion.

5.2.2. Lower ELD

The Lower ELD within the interior crater could be the product of lacustrine, fluid expulsion, or aeolian deposition. However, the deposit contrasts greatly from the main mound in size, composition, and morphology. This indicates that regardless of their deposition, the two ELDs have had different alteration histories. The two ELDs could be from the same depositional event or from separate events that either occurred simultaneously or separately. In a lacustrine scenario, layering is expected to be horizontal. Since the layer attitudes of the Lower ELD are not horizontal, a lacustrine deposition would have been followed by some collapse or subsidence. In an aeolian depositional scenario such as ash fall, ash could have been deposited upon water or ice that filled the crater (Fueten et al., 2014; Schmidt et al., 2018). However, the small extent and lack of ELDs observed close to the crater rim implies that either deposition was somehow confined to the central area of the crater or a very significant amount of the deposit has been eroded. The katabatic winds process (Kite et al., 2013) may help to overcome these discrepancies, however does not fit the Lower ELD well because it is not a mound. Fluid expulsion is an attractive scenario as it can explain the centralized location and the hydrated mineralogy. However, we recognize that hydrated mineral formation and layer deposition are not necessarily achieved by the same process.

Alternatively, the Lower ELD could be thought of as allochthonous blocks that were originally part of the ELD Mound which later broke away and fell into the interior crater. Layer attitudes are highly variable and the smooth material that truncates layering may in fact be deposited between separated blocks of layering. The blocks themselves appear to be oriented in a disordered way. This gives the impression that these blocks were brought into the interior crater from toppling, carried by landslides, or even turbiditic slides under water. However, given the distance from the Lower ELD and the ELD Mound, as well as the height of the crater rim that separates them, from a sheer geometrical perspective it is difficult to explain how sections of the main mound were detached and carried into the interior crater. The interior crater rim has no major splitting or deformation. To overcome a crater rim that is nearly 500 m high is impossible unless the ELD Mound originally extended to the rim and towered above it. However, the rim itself does not indicate any type of rock fall or erosional features that would be expected if large amounts of debris were tumbling over it and down the side. Furthermore, there are no traces of

the deposit directly below the rim or any indication that material was moved from here to the center of the crater over 10 km away. Thus, we argue the location of the Lower ELD is the original site of its formation.

We suggest that there were at least two depositional events within the interior crater: (a) the deposition of the layered deposits and (b) the deposition of the smooth material. Layer deposition could have been either the same event as the deposition of the ELD Mound or a separate event. If they were deposited from the same event, the thinner layering and lack of observed thinning and thickening sequences of the Lower ELD demonstrate a lower energy environment existed within the interior crater than elsewhere in Becquerel. Alternatively, layering within the interior crater might represent a late deposition as water activity decreased and focused only in the deepest areas. The thin layering is not observably laterally continuous like layering in the ELD Mound, which means layer formation in the Lower ELD from fluid expulsion is a more acceptable possibility than it is for the ELD Mound. The deposition of the smooth material occurred as fluid expulsion from below the layering which utilized weak areas and ultimately separated entire sections of the layering.

5.2.3. Hydrated Minerals

Our analyses show that not only are there extensive hydrated minerals, but that the Lower ELD and the ELD Mound have unique and differing compositions. The Lower ELD has two different mineral signatures, characterized by layered areas of Al-clay or hydrated silica, and a smooth material with a unique 2.29 μm absorption indicating a Mg/Fe clay. Conversely, the ELD Mound displays a mineral signature indicative of monohydrated sulfates. The Lower ELD is characterized by an absorption at 1.9 μm and a unique absorption at 2.29 μm with a distinct spectral slope in the 2.3–2.32 μm. This is indicative of vermiculite (a clay) (Michalski & Niles, 2010) and spectra match well with the CAT library spectrum Vermiculite LAVE01 (Figure 4). The combination of absorptions at 2.1 and 2.4 μm observed in the spectra of the ELD Mound is a common diagnostic of monohydrated sulfates (Gendrin et al., 2005), such as kieserite. Spectra match fairly well with the CAT library spectrum Kieserite F1CC15 (Figure 2b) and less with a Mg-polyhydrated sulfate due to the broad absorption between 1.90 and 2.10 extending further to 2.10 than would be expected in a polyhydrated sulfate.

The possibility of the presence of hydrated silica associated with the Lower ELD has several implications to the post layer formation environment within the interior crater. Particularly, estimates of the amount, duration, and temperature of water. Geological settings can be grouped into three possibilities: (a) Acidic dissolution of basalts (as proposed by Milliken et al. [2008], for Valles Marineris and Noctis Labyrinthus), where fluids with pH < 4 would evaporate and deposit mineral sequences such as opaline silica stratigraphically below Fe-sulfates. In this scenario, we would expect the absence of volcanic vents that would suggest a hydrothermal environment. It is then suggested that inverted channels and nonstochiometric jarosite could constitute evidence for non-volcanic, non-hydrothermal processes. In such scenario, we would also expect an association of minerals typical of acidic environments: Al-sulfates (e.g., Alunite), Fe-sulfates (e.g., Jarosite), Pyrite, Kaolonite, poorly crystalline clays, and a variable amount of Ti (Sun & Milliken, 2018). (b) A hydrothermal environment where the proximity to volcanic deposits and/or vents, the porous and brecciated micro-texture, and the stratiform distribution of silica-rich outcrops suggest that hydrothermal processes may be responsible for the deposition of hydrated silica (e.g., Ruff et al., 2011, in Gusev crater). (c) The hydrated silica is diagenetic alteration product where opal-A (amorphous) is alterated into opal-CT (paracrystalline) (Viviano-Beck et al., 2014). The level of crystallinity in opal is directly proportional to the water-rock interaction: the amorphous phase (opal-A) is typical of environments where water did not last long, while more and more crystalline forms of opal (opal-CT or quartz) suggest that water persisted over a long span of time.

Noise within spectra of the ELD Mound implies a significant amount of dust interference, however spectra from lower elevations of the mound tended to be more pristine. Conversely, interference was nearly non-existent within the Lower LED. This implies dust deposition favors places of higher altitude. The contrast between low dust interference in lower sections and high dust interference in higher sections also implies the rate of dust deposition is higher than the rate of Aeolian erosion.

Hydrated mineral formation within these types of deposits has been heavily debated with the general synopsis stemming from two possibilities, that hydrated minerals are either syndepositional or post-depositional. Sources of water, sulfur, and the sediments themselves are not agreed upon. Ash deposition into water (e.g., Chapman, 2002; Fueten et al., 2014; Hynek et al., 2003; Lucchitta, 1990), a fluctuating groundwater table that evaporated and altered/cemented pre-existing eolian or volcanic sediments, syndeposition of dust with sulfuric acid and acid snow (Niles & Michalski, 2009), or cooling hydrothermal water (Al-Samir et al., 2017; Noel

et al., 2015) have all been proposed as plausible origin for the sulfate-rich layered mounds of Valles Marineris. The ELD Mound is characterized by monohydrated sulfate detections, with no signs of a massive transition to polyhydrated sulfates as seen in Valles Marineris (Fueten et al., 2017; Schmidt et al., 2018). It has been proposed previously that this could be a product of the dehydration of polyhydrated sulfates, and/or burial diagenesis (e.g., Mangold et al., 2008; Roach, Mustard, Swayze, et al., 2010; Wang et al., 2016). The opposite could occur during prolonged periods of exposure to ice where kieserite has the potential to transform to a polyhydrated sulfate (Roach, Mustard, Lane, et al., 2010), however no signs of glacial activity were observed within Becquerel which agrees with the observed dominance of monohydrated sulfates. If the hydrated minerals formed post-depositionally, the presence of sulfur implies an ash fall origin (ash is sulfur-rich) or sulfur-rich water could have altered pre-existing sediments through continued fluid expulsion. If the depositional environment present in Becquerel was similar to the combined lacustrine and groundwater upwelling environment proposed to have existed in Juventae Chasma (Al-Samir et al., 2017), then hydrated sulfates could be the bulk composition of the ELD Mound, rather than a surface veneer. Regional layer thickness measurements of ELDs across western Arabia Terra (Annex & Lewis, 2020; Schmidt et al., 2021) conflicts with ash fall characteristics and known locations of volcanic provinces. Thus, sulfur-rich water in the system is more probable. Interestingly, this makes Becquerel a great location for discussing and applying concepts on the evolution of sulfur-based life forms.

The elevation difference between the two deposits was likely a strong influence on the formation of phyllosilicates in the Lower ELD. The lower elevation may have meant that it was more susceptible to hydrothermal activity, and the possibility of a persistent water level at an elevation between it and the large mound strongly fits with the observations. Vermiculite is a common product of mafic alteration and could have formed from hydrothermal alteration of micas present in the interior crater or by the leaching of micas during a later fluid expulsion event (Shirozu & Bailey, 1966). We propose that the non-layered smooth material found amongst the Lower ELD is vermiculite, and as mentioned previously, was deposited later possibly through weak points or fractures within layered sections. It isn't clear if the clay deposition formed fractures in the Lower ELD layering due to fluid pressure from below or the clay deposition used pre-existing fractures. The event which deposited the smooth material may have also altered the layering to an Al-clay or hydrated silica. The presence of hydrated silica might also imply an environment similar to Mawrth Vallis, where an Al/Si-rich unit has been identified (Bishop et al., 2008).

5.2.4. Duality of Aeolian and Aqueous Influence

5.2.4.1. Review of Depositional Processes

We suggest that a complete catalog of the depositional processes and settings which hold merit in Becquerel includes: lacustrine, springs, mixed lacustrine/springs, mud volcanism, diapirism, platform evaporites, ash fall, aeolian dust/dusty glacier, and katabatic winds (Tables 1 and 2). This catalog includes processes previously proposed for ELDs in Arabia Terra (presented in the Introduction section), as well as the aeolian deposition onto ice process previously proposed for layered mounds in Valles Marineris by Michalski and Niles (2012) which we refer to as "dusty glacier." Additionally, we suggest that in the case of Becquerel a process similar to what forms platform evaporites on Earth (Warren, 2010) should be considered a possibility as well. Due to the combination of the proximity of the putative ocean 600 km to northwest (Di Achille & Hynek, 2010; Rodriguez et al., 2016; Webb, 2004) and the regional layer thickness trend of western Arabia Terra (Schmidt et al., 2021), a setting where platform evaporates forming at the sub-sea level in a type of marine-seepage lagoon setting (Warren, 2010) is an idea included in the catalog of depositional possibilities for assessment. We recognize that many of these processes can also occur during alteration, and thus mixed processes in Becquerel's history can be posited as well. By comparing and contrasting the observed features of the ELDs with specific features produced from these depositional possibilities, the formation of both ELDs can be further constrained (Tables 1 and 2). This assessment essentially grades all depositional possibilities in an effort to reveal how consistent they are in the setting of Becquerel.

Each of the possible depositional processes has unique implications on the geological setting and evolution of the ELDs (Table 1). These are either environmental requirements which are necessary to sustain the depositional process, or a specific result that is expected if the depositional process occurred. These implications are essentially the base expectations and consequences of the possible depositional processes, which provide a framework for conceptualizing their existence in Becquerel. In the case of a strictly lacustrine deposition, it is implied that the water level would have reached a minimum elevation of −2,700 m, which represents the current height of the

Table 1
A Catalog of the Possible Depositional Processes and Settings That Could Have Occurred in Becquerel (Column 1) and the Unique Implications Each Would Have

Depositional process/setting	Implications
Lacustrine	Water level reached ≥−2,700 m elev. (the height of the ELD Mound)
Springs	Requires sufficient fluid pressure to reach the ELD Mound top
Mixed Lacustrine and Springs	Spring activity feeds/contributes to water level
	Spring activity provides catchment area for ELD Mound placement
	Spring activity more readily influences the Lower ELD due to elevation
Mud Volcanoes	Presence of massive quantiy of less dense material below
Diapirism	Presence of massive quantity of salt deposits below
Platform Evaporites	Existence of ocean
Ash Fall	>37,000 km^3 eroded material
Aeolian Dust/Dusty Glacier	>37,000 km^3 eroded material
Katabatic Winds	Presence of interior crater's ridge has no effect on wind transport from the north

ELD Mound. In a spring deposition, it is implied that there was sufficient fluid pressure to reach the uppermost sections of the ELD Mound. If there was mixed lacustrine and spring activity, then it is implied that spring activity contributed to the influx of water in the lake, provided a catchment area for aeolian sediment if/when water level was very low or non-existent, and had a stronger influence on the Lower ELD than on the ELD Mound due to the lower elevation of the Lower ELD. If mud volcanoes were at all an active process, it implies a massive quantity of less dense material below the ELDs (Brown, 1990; Kopf, 2002; Morley & Guerin, 1996). In the case of diapirism, it is implied that a massive quantity of salt deposits were present or formed during ELD evolution. In a scenario in which the ELDs are platform evaporites, it is implied that an ocean shoreline at the boundary of western Arabia Terra and Chryse Planitia existed during their formation. In the instance of an ash or dust fall deposition either in a dry basin or upon ice (i.e., "dusty glacier"), the upwards of 37,000 km^3 may have been eroded from the crater given that the aeolian deposition filled the entire crater. Lastly, if katabatic winds were a depositional process, then the presence of the interior crater's rim did not affect the transport of sediment since layering is evenly continuous throughout the ELD Mound (apart from the later deformational features), even on its north side adjacent to the interior crater rim.

Apart from these implications, th e depositional processes can be evaluated by specific observations from the ELDs (Table 2). By matching certain geological features which are expected from each depositional process, a first order probability of the existence of each process can be determined. These geological features include: laterally continuous layering, thinning and thickening sequences, indications of water level, particle size and sorting, conical shapes or small mounds, composition (i.e., presence of hydrated minerals), hydrothermal alteration (i.e., presence of minerals that can be formed in hydrothermal environments), non-layered material, faulting/fracturing, infilled fractures, doming, draping structures, sulfur content, change in bed thicknesses in specific direction (i.e., indicating proximal/distal relationship to source), glacial/periglacial morphology, deposit shape (i.e., circular, ellipsoidal, or patchy), outward radial dips, and spatial placement of the deposit within the crater. Each of these geological features are given either "Yes," "No," "Possible," or "Inconclusive" to assess which depositional processes have the most compatibility (Table 2).

A lacustrine process would produce laterally continuous layering and signs of water level within Becquerel. Laterally continuous layering is observed in the ELD Mound, however due to the smooth material truncating layering in the Lower ELD (Figures 3 and 4, also see Supporting Information S1 for further examples), it is not certain if the layering was originally laterally continuous. Water level is indicated by the stepped deltas within the interior crater. It is possible that grain sizes of the ELDs are small, even silt sized, however a grain size less than 30 cm is the best assertion since they cannot be resolved in HiRISE images. Without insitu analysis, grain properties such as sorting and size cannot be determined, however the Mars Science Laboratory (MSL) has shown that grains of layered outcrops in Gale crater are akin to those of lacustrine environments (Edgar et al., 2020;

Grotzinger et al., 2014; Rivera-Hernández et al., 2020). Additionally, a major problem in a lacustrine deposition is that one would expect to see ELD dispersed evenly upon the crater floor (Day et al., 2019), which is not observed in Becquerel.

Spring deposition would produce conical shapes, hydrated minerals, non-laterally continuous layering, as well as material void of layering. Conical shapes (i.e., small mounds) are present in both the Lower ELD and the ELD Mound (Figures 1, 2, 13, and 15), as well as hydrated minerals. As discussed, the ELD Mound has laterally continuous layering, whereas the Lower ELD has its layering truncated by the smooth material. Both ELDs have areas void of layering, however these areas are much more pronounced in the Lower ELD. Mixed lacustrine and spring deposition would have areas of layered and non-layered material, but unlike the Lower ELD, it is not apparent from our observations if areas void of layering within the ELD Mound are separate material. Both ELDs do have infilled fractures, something that would be expected in a spring environment or mixed lacustrine and spring environment.

Observations do not give much support to a process of mud volcanism in Becquerel. Apart from identifications of hydrated silica and vermiculite in the Lower ELD, which can be produced by hydrothermal alteration, the observed conical shapes do not have pits like those observed elsewhere in Arabia Terra (Pondrelli et al., 2011).

As mentioned previously, diaprism is an unlikely process to deposit the observed layering, however could have been a process contributing the evolution of the ELDs. Diaprism would produce hydrated sulfates, faults or fractures, and doming. These are all observed in the ELD Mound, whereas only faults and fractures were observed in the Lower ELD. This means that if diaprism was ever an active process in Becquerel, it was only affecting the ELD Mound.

In a platform evaporite setting, hydrated sulfates and thinning/thickening sequences would be produced (Warren, 2016). Thinning and thickening sequences can be produced due to shallowing-up evaporite cycles and the peritidal zone (Aigner & Bachmann, 1989; Warren, 2016). Furthermore, the proximity to the putative ocean shoreline (600 km) is an acceptable distance for this type of setting to form (Warren, 2010, 2016). However, hydrated sulfates were not identified within the Lower ELD. As discussed previously, layer thicknesses within the Lower ELD do not resolve thinning and thickening sequences, only that the thickness does increase slightly with elevation.

Aeolian deposition is a strong candidate process for ELD formation in Becquerel. However, ash fall is not supported by our observations. No draping structures or folding of any kind were observed. The shapes of the ELDs do not indicate any source direction, nor do the layer thicknesses. As discussed, non-radial outward dips are not agreeable with the katabatic winds model (Kite et al., 2013) and the off center location of the ELD Mound makes an airfall deposition problematic. If layers were formed by aeolian deposition, deposit remnants should be found elsewhere around the crater as other craters in Arabia Terra have been described (Annex & Lewis, 2020; Murana, 2018; Pajola et al., 2022; Pondrelli et al., 2019; Schmidt et al., 2021), not localized to a specific location. Likewise, aeolian dust collected onto seasonal ice (Michalski & Niles, 2012) could produce thinning and thickening sequences (Lewis & Aharonson, 2014), however the lack of glacial or periglacial morphology in the study area means that ice likely did not play a major role in the deposition. However, it might be possible that such thinning and thickening sequences could be produced in a lacustrine setting where the water level is fluctuating (Cadieux & Kah, 2015; Schmidt et al., 2021).

Broadly speaking, we argue that deposition must either be aeolian with water activity influencing the location of the mound (i.e., fluid expulsion at a point directly under the mound which favored the retention of sediment and lithification of layers), or strictly fluid expulsion. In the event of an aeolian deposition of the ELDs, the mound's location is not easily explained without significant erosion. However, this remains problematic because the ELD Mound is over 60 times larger than the Lower ELD, yet should be more susceptible to erosion due to its higher elevation. In the event of deposition by fluid expulsion, the continuous and mostly uniform layers are not easily explained. Based on layer thickness differences between the ELD Mound and the Lower ELD, in combination with specific water elevation ranges observed in the fan shaped landforms (Figure 14) the geology of Becquerel clearly points to a strong influence of water whether layer formation was aeolian or fluid expulsion dominated.

Table 2
A Catalog of the Possible Depositional Processes and Settings That Could Have Occurred in Becquerel (Column 1) and the Expected Geological Features That Each Depositional Process or Setting Would Form (Column 2)

		Result	
Depositional process/setting	Expected geological features	Lower ELD	ELD Mound
Lacustrine	Laterally continuous layering	Possible	Yes
	Water level indicators	Yes	Yes
	Small particle size	Possible	Possible
	Well sorted	Inconclusive	Inconclusive
Springs	Conical shapes	Yes	Yes
	Hydrated minerals	Yes	Yes
	Non-laterally continuous layering	Possible	No
	Material void of layering	Yes	Yes
Mixed Lacustine and Springs	Juxtaposition of layerless and layered materials	Yes	No
	Infilled fractures	Yes	Yes
Mud Volcanoes	Conical shapes with pits	No	No
	Hydrothermal alteration	Yes	No
Diapirism	Hydrated sulfates	No	Yes
	Faulting/fracturing	Yes	Yes
	Doming	No	Yes
Platform Evaporites	Hydrated sulfates	No	Yes
	Proximity to shoreline	Yes	Yes
	Thinning/thickening sequences	Possible	Yes
Ash Fall	Draping structures (e.g. folds)	No	No
	Sulfur content	No	Yes
	Shape indicating source direction	No	No
	Bed thicknesses prox/distal response	No	No
Aeolian Dust/Dusty Glacier	Thinning/Thickening sequences	Possible	Yes
	Glacial/periclacial morphology	No	No
Katabatic Winds	Presence of layered mound	No	Yes
	Outward radial dips	No	No
	Center of crater placement	Yes	No

Note. Each depositional processes is appraised based on the observations by placing "Yes," "No," "Possible," or "Inconclusive" for the Lower ELD and ELD Mound (column 3).

5.2.4.2. Proposed Process

We find that a process of fluid expulsion is necessary to explain all observations without creating an overly complicated scenario. This method can account for layer formation, clay intrusion along faults of the Lower ELD, aqueous alteration, mound deformation, spatial location of the ELD Mound, lack of ELDs present elsewhere around the crater, and the problem of eroding tens of thousands of cubic kilometers of material. Grindrod and Balme (2010) showed that the hydraulic pressure required in large mounds (in the case of that study the 8 km tall Hebes Mensa) was too high, but with the much smaller 800 m tall ELD Mound, the hydraulic pressure can be much less. Furthermore, events in Becquerel might have had higher pressures if aided by heat which is a likely possibility due to the presence of vermiculite and hydrated silica.

Despite this, spring deposits do not match well with the existence of the laterally continuous layering in the ELD Mound. Thus, although fluid expulsion can be demonstrated to have had a major role in both the formation and alteration of these ELDs, the deposition of layering in at least the ELD Mound by springs does not match well

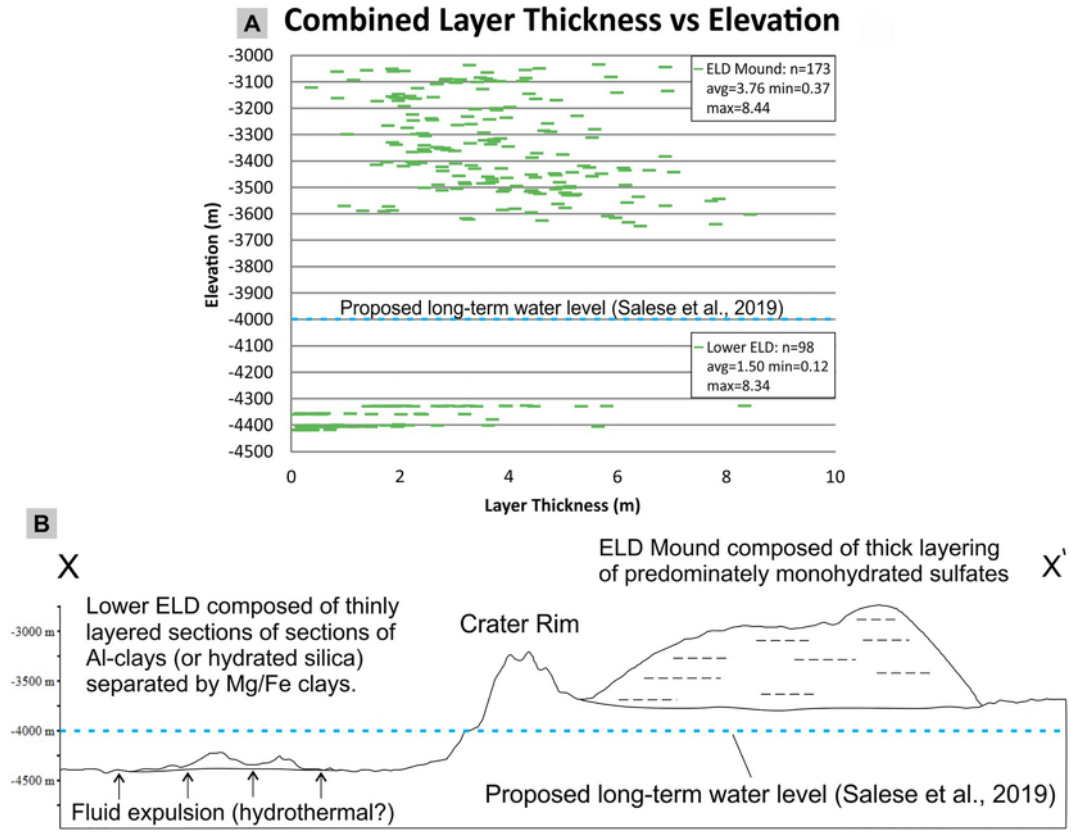

Figure 16. Combined layer thicknesses and cross-section in reference to the proposed long-term water level by Salese et al. (2019).

with the observations. Aeolian or lacustrine deposition are more attractive alternatives to produce the observed layering, however require extensive erosion that other ELD mounds in Arabia Terra (e.g., Crommelin, Firsoff, and Henry) are lacking. They can still be invoked, but the presence of fluid expulsion at the location of the ELD Mound (as to produce a catchment area) helps explain the mound location and is an alternative to the erosion volume problem. In an ash fall scenario, we would except to observe a thinning of layering in a preferred direction which would reflect a proximal/distal effect from the source. Although layering does thin southeast to northwest from the ELD Mound to the Lower ELD, there is no known volcanic province to the southeast of Becquerel. Furthermore, Lewis and Aharonson (2014) demonstrated that the observed thinning and thickening sequences do not represent ash deposits because layered ash would be stochastic. As an alternative, dusty glaciers depositing layers overtime over repeated intervals could form the observed layering. However, no glacial morphology was observed in the study area and it isn't clear how this process would create the observed differences between the Lower ELD and the ELD Mound.

In this fluid expulsion scenario, the location of the Lower ELD and the ELD Mound is due to the ability of water to protrude through the crater floor at those specific locations (Figures 16 and 17). Thinning and thickening sequences observed in the ELD Mound might represent changes in fluid pressure and/or degree of water saturation. Thinner layers of the Lower ELD represent a lower energy environment. Maximum layer thickness of both the ELD Mound and the Lower ELD are strikingly similar (8.44 and 8.34 m respectively). This might represent an energy threshold of some kind related to the upwelling water. All dips >8° are associated with faults or sliding and are thus not considered to be syndepositional features. Layer attitudes do not suggest draping on a pre-existing topography as proposed by Schmidt et al. (2018). The absence of folding within the ELD Mound also indicates that there wasn't a significant compaction process after deposition.

Timing and size difference between the Lower ELD and the ELD Mound are not easily explained in any scenario. Given that the ELD Mound was formed after the formation of the interior crater, both deposits had the opportunity to form at the same time. However, it is possible that one was deposited before the other if upwelling

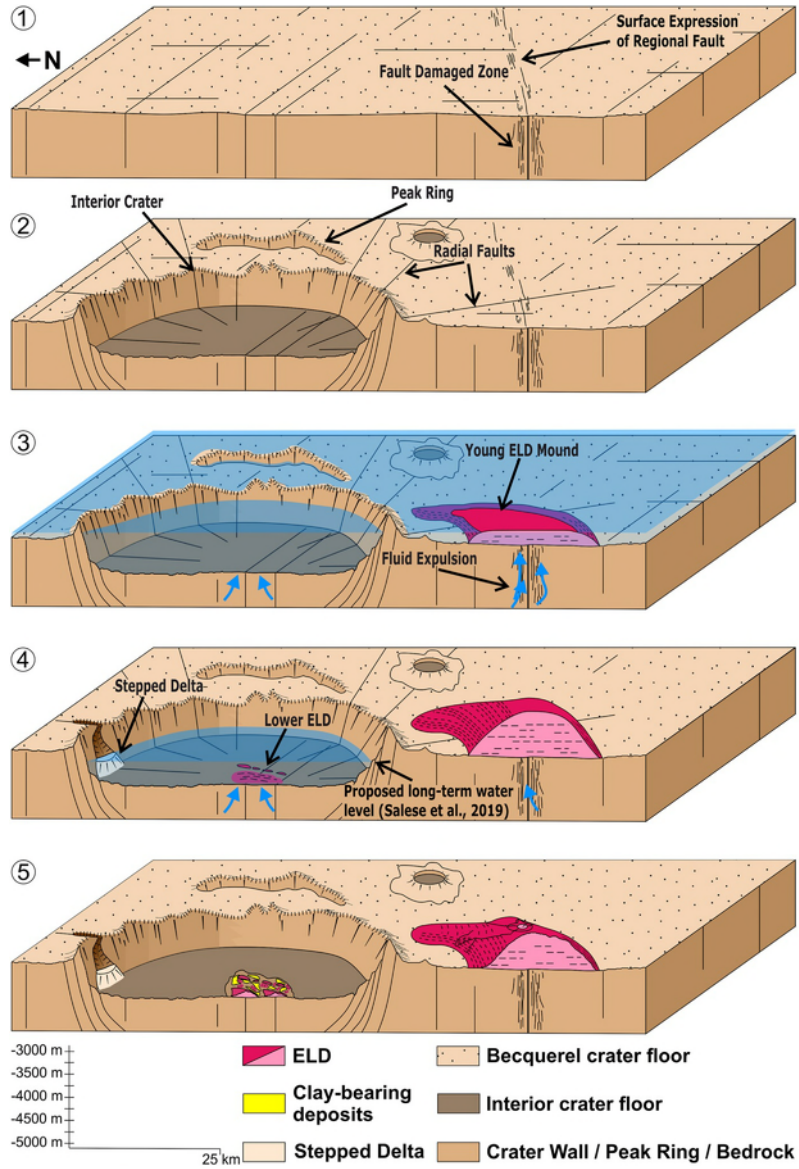

Figure 17. Proposed stages of the depositional history in Becquerel. Cross section aided by High Resolution Stereo Camera derived topography (V.E. = 6X).

water was somehow blocked underneath one of them and then consequently redirected to the other. For instance, perhaps it was the path of least resistance for water to propagate from below the ELD Mound, but after time the mound became too large to accommodate hydraulic pressure and water then favored to propagate from below the Lower ELD. Becquerel's proximity to the possible ancient ocean also brings the possibility of a platform evaporate setting involving ocean water circulation which propagated through faults underneath both ELD deposits. However, fluid expulsion is not dependent on the existence of an ocean. Perhaps the key take-away from our work is that even if the ELDs were formed from aeolian deposition, the differences in layer thickness and composition between the two, coupled with their 700 m elevation difference, which passes through the proposed long-term water level of −4,000 m (Salese et al., 2019) and is further supported by the same elevation of the stepped deltas, is very strong evidence that water activity played a crucial role in the geological history of Becquerel (Figure 16).

Our favored idea is that the position of the ELD Mound is the product of the intersection of a radial fracture system (related to the interior crater impact event) and the presence of a pre-existing regional fault and its damaged zone (Caine et al., 1996; Ruj et al., 2017), which creates the required permeability.

After a detailed work on the presence of hydrated minerals in Becquerel, Koeppel et al. (2022) concluded on the basis of numerical modeling of THEMIS images of ELDs (referred to in the article as SBLDs) that the contribution of water (if any) was minimal. This was based on the resulting, relatively lower than expected, cohesion of hydrated mineral bearing sediments. This could imply that the ELDs did not endure much time under the influence of aqueous conditions. More contribution to this uncertainty is required, including the difference in grain sorting produced by the various possible aqueous environments that could have been present (e.g., beach with respect to deep water), as well as the relation of wind over time to both the dust deposition and the cooling effect that wind adds to the thermal inertia computation. Results from our study further leave open the role that water played during the formation and evolution of these deposits because we provide structural and geomorphological observations in favor of a significant contribution of aqueous activity in the system.

5.3. Proposed Sequence of Events

We propose a sequence of events to describe the evolution of Becquerel based largely on three conjectures, which when brought together might achieve in replicating all of our observations: (a) The circulation of water is influenced by a radial fault system formed from the interior crater impact event. (b) The position of the ELD Mound is the product of the intersection of the radial fracture system and the presence of a pre-existing regional fault and its damaged zone (Caine et al., 1996), which creates the required permeability along the segment closest to the interior crater. The proposed fault, though not directly observable, would be very old and covered by regolith. (c) ELD deposition, hydrated mineral formation, and the stepped delta represent different periods of water activity.

Crater-related fault structures have been described previously (Head & Mustard, 2006; Osinski & Spray, 2005) which form during and after the impact event. Such fracture systems have important implications on a potential planet-wide groundwater system (Head & Mustard, 2006; Salese et al., 2019), as well as hydrothermal activity (Osinski et al., 2005). Head and Mustard (2006) presented similar impact structures, in this case breccia dikes, which could reach 500 m in depth. On Earth, impact structures are well-known for their hydrocarbon implications, in particular the Red Wing Creek structure, famous for oil propagation through the impact fracture system of the crater (Donofrio, 1981; Koeberl et al., 1996). Fault damage zones can provide a porous medium from fault related fractures which act as conduits for fluid flow (Caine et al., 1996). Thus, we see no reason why crater-related faults cannot also provide the pathways for fluid expulsion also in Becquerel.

Based on our observations, the following sequence of geological events is proposed and simplified into five stages (Figure 17):

1. The floor of Becquerel crater. At this time only the regional fault and a few minor faults exist. (Early-Middle Noachian)
2. An impact event occurs forming the interior crater, a peak ring, and a radial fault system. (Late Noachian)
3. Fluid expulsion begins with the more intensity along the fault damaged zone due to least resistance and the crater is then filled with water by groundwater table oscillations predicted by Andrews-Hanna et al. (2010) which may eventually established a lake. Deposition of the ELD Mound begins by repeated fluid expulsion pulses. During this time, the water level might have fluctuated between the long-term level of −4,000 m (Salese et al., 2019) and −2,700 m. However, we argue it is not necessary that Becquerel contained a lake, water may have remained predominately within the interior crater throughout time and periodically pooled in areas of Becquerel. We mean only to propose that the elevations −4,000 m and −2,700 m provide good anchor points for indicating a possible range of water level fluctuation. At the least, some volume of water is required to be contained in Becquerel and drain into the interior crater in order to later form the stepped deltas. (Late Noachian-Early Hesperian)
4. As the ELD Mound is formed, the water table stabilizes to an elevation range of −4,000 to −4,100 m, perhaps due to lower fluid pressure. This water level is maintained for an extended period of time which results in the long-term exposure of the ELD Mound. During this time, evaporation alteration occurs in the main mound and hydrated sulfates are formed. Additionally during this time, the two stepped deltas form and continued spring activity below the ELD Mound, coupled with the evaporitic setting within the crater, create conditions which deformed the ELD Mound. The sapping channel associated with the larger stepped delta likely formed along one of the impact related radial faults. (Early Hesperian).
5. Internal diapirism and swelling from the creation of evaporates inside the ELD Mound begin to form normal radial faults and induce large scale movements of intact sections down slope upon slip surface lubricated by

water and/or salt layers. The central collapse structure is also formed. We suggest at this point, deposition of the Lower ELD begins due to a shift in the preferred fluid pathway, perhaps due to a type of hydraulic head phenomena, but it never becomes the size of the ELD Mound due to reduced fluid intensity. This reduced fluid intensity results in thinner layering. The water table then lowers further, fluctuating and creating alternating wet and dry periods within the interior crater forming hydrated sulfates. As the water table falls just below the interior crater floor, fluid expulsion possibly influenced by deeper hydrothermal activity, forces water and material upwards through weak points in the Lower ELD which deposits clays and alters pre-existing layers (Early-Middle Hesperian). Lastly, aeolian erosion becomes the main process acting on these deposits and produces the N-S trending yardangs observed on the south side of the main mound. (Late Hesperian-present).

6. Conclusions

Becquerel crater provides a unique opportunity in Arabia Terra to observe the effects that the elevation has on the alteration of layered deposits. The complex subaqueous and/or aeolian deposition was most likely followed by aqueous alteration episodes. The over 700 m elevation difference between the two ELDs produced two diverse depositional and alteration environments. Evidence of protracted fluid expulsion during Becquerel's evolution shows that the layered deposits of Arabia Terra are extremely diverse from crater to crater. While many ELDs have been previously proposed to likely have been formed from an aeolian deposition, water activity is a necessity in Becquerel given the overwhelming evidence from deposit geometries and spatial placements, volume constraints on erosion, layer attitudes, and the different hydrated minerals. Therefore, Becquerel represents a point of regional change in how layers form in Arabia Terra. We also find that evidence of sustained fluid expulsion in the past, possibly hydrothermal, makes Becquerel crater a superior candidate for future missions searching for traces of ancient life, particularly those that interact with sulfur compounds as it is observed today in the mid-ocean ridges of our planet. Furthermore, the reactivation of regional faults as fluid pathways, as we propose, reveals new possibilities in interpreting the geological history of isolated basins.

The difference in composition between two ELDs in close proximity to each other, yet residing at different depths, supports both the higher probability of clay and hydrated silica formation with depth, as well as the predicted −4,000 m water-level (Salese et al., 2019). Furthermore, the existence of deltas just below this water level bolsters further the significance of this elevation.

The structural setting is dominated by an extensional (or transtensional) NW-SE trend, but also some E-W discontinuities, probably exploiting the weakness of the bedding surface. On the top of the mound the circular feature of the depression relates to the collapse and the radial structures derive from domal-type emplacement. This evidence led us to the hypothesis of an internal collapse, likely due to a mud/salt diapir rising from depth. Interestingly, nearby Trouvelot crater has a similar oblique shaped layered mound adjacent to an interior crater as well. Perhaps the existence of an interior crater is an underlying reason for certain intracrater deposits by providing an increase in fluid conduits by the associated radial fracturing.

Future work involves a combination of projects that require data not yet available, and the utilization of existing data: (a) more HiRISE coverage of the interior crater and exploring the depositional relationship between it and the main mound. (b) Reliable ground penetrating radar to explore diapirism origins and deep faulting that could have been used as conduits for fluid expulsion. (c) Comparing to the layered deposits of Gale Crater. (d) Mapping all faults within the ELD Mound and determining stress states and direction. (e) Comparing the clays of the Lower ELD to those in Mawrth Vallis and nearby McLaughlin crater. (f) Comparing the ELD Mound to the nearby mound in Trouvelot. (g) Careful analysis of internal layering composition to unravel the subaqueous versus aerial environment of deposition.

Data Availability Statement

The orbital data sets HiRISE, CTX, and HRSC used in this study are available from the Planetary Data System (PDS) node at their respective archives listed and linked here: https://pds.nasa.gov/datasearch/subscription-service/SS-20150302.shtml (Malin, 2007; Malin et al., 2007; McEwen, 2006; McEwen & Team, 2009;

McEwen et al., 2005) and https://www.cosmos.esa.int/web/psa/mars-express (Heather et al., 2013a, 2013b). Satellite images and topography were processed in-house with ISIS (Integrated Software for Imagers and Spectrometers) available online at https://isis.astrogeology.usgs.gov. Processed data was projected into a Global Mapper 15.0 GIS software environment. Data for this work including CRISM observations, .roi files for use in ENVI, layer thickness spreadsheets and point coordinates, layer attitude statistics and point coordinates, DEMs, as well as a free version of Orion are publicly available at: https://doi.org/10.5281/zenodo.6560965 (Schmidt, 2022).

Acknowledgments

A special thanks to Dr. Frank Fueten and Dr. Laetitia Le Deit for ongoing insightful conversations about layered deposit hypotheses. We would like to acknowledge ESA, DLR, FU-Berlin, and the HRSC Science Team for the joint effort in processing the HRSC DEM of the MC-11 quadrangle of Mars. We would like to thank all teams involved with image acquisition and on-going maintenance of these orbiters: the MRO and HRSC teams. This work was funded by the Dipartimento di Ingegneria e Geologia GeoQuTe Lab (Laboratorio di Geodinamica Quantitativa e Telerilevamento) of Roma Tre University, the Department of Physics and Earth Sciences of Jacobs University Bremen, and the Diparimento di Ingengneria e Geologia della Università degli Studi "G. d'Annunzio" Chieti-Pescara".

References

Aigner, T., & Bachmann, G. H. (1989). Dynamic stratigraphy of an evaporite-to-red bed sequence, Gipskeuper (Triassic), southwest German Basin. *Sedimentary Geology*, *62*(1), 5–25. https://doi.org/10.1016/0037-0738(89)90098-5

Allen, C. C., & Oehler, D. Z. (2008). A case for ancient springs in Arabia Terra, Mars. *Astrobiology*, *8*(6), 1093–1112. https://doi.org/10.1089/ast.2008.0239

Al-Samir, M., Nabhan, S., Fritz, J., Winkler, A., Bishop, J. L., Gross, C., & Jaumann, R. (2017). The paleolacustrine evolution of Juventae Chasma and Maja Valles and its implications for the formation of interior layered deposits on Mars. *Icarus*, *292*, 125–143. https://doi.org/10.1016/j.icarus.2016.12.023

Anderson, R. C., Dohm, J. M., Haldemann, A. F. C., Pounders, E., Golombek, M., & Castano, A. (2008). Centers of tectonic activity in the eastern hemisphere of Mars. *Icarus*, *195*(2), 537–546. https://doi.org/10.1016/j.icarus.2007.12.027

Andrews-Hanna, J. C., Phillips, R. J., & Zuber, M. T. (2007). Meridiani Planum and the global hydrology of Mars. *Nature*, *446*(7132), 163–166. https://doi.org/10.1038/nature05594

Andrews-Hanna, J. C., Zuber, M. T., Arvidson, R. E., & Wiseman, S. M. (2010). Early Mars hydrology: Meridiani playa deposits and the sedimentary record of Arabia Terra. *Journal of Geophysical Research*, *115*(E6), E06002. https://doi.org/10.1029/2009JE003485

Annex, A. M., & Lewis, K. W. (2020). Regional correlations in the layered deposits of Arabia Terra, Mars. *Journal of Geophysical Research: Planets*, *125*(6), e2019JE006188. https://doi.org/10.1029/2019JE006188

Baker, V. R., Strom, R. G., Gulick, V. C., Kargel, J. S., Komatsu, G., & Kale, V. S. (1991). Ancient oceans, ice sheets and the hydrological cycle on Mars. *Nature*, *352*(6336), 589–594. https://doi.org/10.1038/352589a0

Beyer, R. A., Alexandrov, O., & McMichael, S. (2018). The Ames Stereo Pipeline: NASA's open source software for deriving and processing terrain data. *Earth and Space Science*, *5*(9), 537–548. https://doi.org/10.1029/2018ea000409

Bibring, J.-P., Langevin, Y., Mustard, J. F., Poulet, F., Arvidson, R., Gendrin, A., et al. (2006). Global mineralogical and aqueous Mars history derived from OMEGA/Mars Express data. *Science*, *312*(5772), 400–404. https://doi.org/10.1126/science.1122659

Bishop, J. L., Dobrea, E. Z. N., McKeown, N. K., Parente, M., Ehlmann, B. L., Michalski, J. R., et al. (2008). Phyllosilicate diversity and past aqueous activity revealed at Mawrth Vallis, Mars. *Science*, *321*(5890), 830–833. https://doi.org/10.1126/science.1159699

Bishop, J. L., Gross, C., Danielsen, J., Parente, M., Murchie, S. L., Horgan, B., et al. (2020). Multiple mineral horizons in layered outcrops at Mawrth Vallis, Mars, signify changing geochemical environments on early Mars. *Icarus*, *341*, 113634. https://doi.org/10.1016/j.icarus.2020.113634

Bishop, J. L., Pieters, C. M., & Edwards, J. O. (1994). Infrared spectroscopic analyses on the nature of water in montmorillonite. *Clays and Clay Minerals*, *42*(6), 702–716. https://doi.org/10.1346/CCMN.1994.0420606

Bishop, J. L., Yeşilbaş, M., Hinman, N. W., Burton, Z. F. M., Englert, P. A. J., Toner, J. D., et al. (2021). Martian subsurface cryosalt expansion and collapse as trigger for landslides. *Science Advances*, *7*(6), eabe4459. https://doi.org/10.1126/sciadv.abe4459

Blue Marble Geographics. (2011). Global mapper [Computer software]. Blue Marble Geographics. Retrieved from https://www.bluemarblegeo.com/global-mapper/

Bridges, J. C., Kim, J. R., Tragheim, D. G., Muller, J. P., Balme, M. R., & Pullan, D. (2008). *Sedimentary rocks in Bequerel crater: Origin as polar layered deposits during high obliquity*. In *Paper presented at 39th Annual Lunar and Planetary Science Conference*. Abstract 1913.

Brown, K. M. (1990). The nature and hydrogeologic significance of mud diapirs and diatremes for accretionary systems. *Journal of Geophysical Research*, *95*(B6), 8969–8982. https://doi.org/10.1029/JB095iB06p08969

Burns, R. G., & Fisher, D. S. (1993). Rates of oxidative weathering on the surface of Mars. *Journal of Geophysical Research*, *98*(E2), 3365–3372. https://doi.org/10.1029/92JE02055

Cadieux, S. B., & Kah, L. C. (2015). To what extent can intracrater layered deposits that lack clear sedimentary textures be used to infer depositional environments? *Icarus*, *248*, 526–538. https://doi.org/10.1016/j.icarus.2014.11.004

Caine, J. S., Evans, J. P., & Forster, C. B. (1996). Fault zone architecture and permeability structure. *Geology*, *24*(11), 1025–1028. https://doi.org/10.1130/0091-7613(1996)024<1025:fzaaps>2.3.co;2

Carr, M. H., & Head, J. W. (2010). Geologic history of Mars. *Earth and Planetary Science Letters*, *294*(3–4), 185–203. https://doi.org/10.1016/j.epsl.2009.06.042

Carter, J., Poulet, F., Bibring, J. P., Mangold, N., & Murchie, S. (2013). Hydrous minerals on Mars as seen by the CRISM and OMEGA imaging spectrometers: Updated global view. *Journal of Geophysical Research: Planets*, *118*(4), 831–858. https://doi.org/10.1029/2012JE004145

Changela, H. G., Chatzitheodoridis, E., Antunes, A., Beaty, D., Bouw, K., Bridges, J. C., et al. (2022). Mars: New insights and unresolved questions–Corrigendum. *International Journal of Astrobiology*, *21*(1), 46. https://doi.org/10.1017/S1473550421000380

Chapman, M. G. (2002). Layered, massive and thin sediments on Mars: Possible Late Noachian to Late Amazonian tephra? *Geological Society, London, Special Publications*, *202*(1), 273–293. https://doi.org/10.1144/GSL.SP.2002.202.01.14

Clark, R. N., King, T. V., Klejwa, M., Swayze, G. A., & Vergo, N. (1990). High spectral resolution reflectance spectroscopy of minerals. *Journal of Geophysical Research*, *95*(B8), 12653–12680. https://doi.org/10.1029/JB095iB08p12653

Clark, R. N., Swayze, G. A., Singer, R. B., & Pollack, J. B. (1990). High-resolution reflectance spectra of Mars in the 2.3-μm region: Evidence for the mineral scapolite. *Journal of Geophysical Research*, *95*(B9), 14463–14480. https://doi.org/10.1029/JB095iB09p14463

Crowley, J., Hook, S., Bridges, N., Thomson, B., Baldridge, A., Brown, A., et al. (2008). *Lacustrine sedimentary rocks from an alkaline environment in Becquerel crater, Arabia Terra, Mars*. In *Joint Meeting of The Geological Society of America* (pp. 195–11).

Day, M., Anderson, W., Kocurek, G., & Mohrig, D. (2016). Carving intracrater layered deposits with wind on Mars. *Geophysical Research Letters*, *43*(6), 2473–2479. https://doi.org/10.1002/2016GL068011

Day, M., Edgett, K. S., & Stumbaugh, D. (2019). Ancient stratigraphy preserving a wet-to-dry, fluvio-lacustrine to aeolian transition near Barth crater, Arabia Terra, Mars. *Journal of Geophysical Research: Planets*, *124*(12), 3402–3421. https://doi.org/10.1029/2019JE006226

Day, M. D., & Catling, D. C. (2020). Potential aeolian deposition of intra-crater layering: A case study of Henry crater, Mars. *Bulletin*, *132*(3–4), 608–616. https://doi.org/10.1130/b35230.1

Deit, L. L., Hauber, E., Fueten, F., Pondrelli, M., Rossi, A. P., & Jaumann, R. (2013). Sequence of infilling events in Gale Crater, Mars: Results from morphology, stratigraphy, and mineralogy. *Journal of Geophysical Research: Planets*, *118*(12), 2439–2473. https://doi.org/10.1002/2012JE004322

de Villiers, G., Kleinhans, M. G., & Postma, G. (2013). Experimental delta formation in crater lakes and implications for interpretation of Martian deltas. *Journal of Geophysical Research: Planets*, *118*(4), 651–670. https://doi.org/10.1002/jgre.20069

Di Achille, G., & Hynek, B. M. (2010). Ancient ocean on Mars supported by global distribution of deltas and valleys. *Nature Geoscience*, *3*(7), 459–463. https://doi.org/10.1038/ngeo891

Di Pietro, I., Ori, G. G., Pondrelli, M., & Salese, F. (2018). Geology of Aeolis Dorsa alluvial sedimentary basin, Mars. *Journal of Maps*, *14*(2), 212–218. https://doi.org/10.1080/17445647.2018.1454350

Donofrio, R. R. (1981). Impact craters: Implications for basement hydrocarbon production. *Journal of Petroleum Geology*, *3*(3), 279–302. https://doi.org/10.1111/j.1747-5457.1981.tb00931.x

Dorn, T., & Day, M. (2020). Intracrater sediment trapping and transport in Arabia Terra, Mars. *Journal of Geophysical Research: Planets*, *125*(9), e2020JE006581. https://doi.org/10.1029/2020JE006581

Dronkert, H., & Remmelts, G. (1996). Influence of salt structures on reservoir rocks in Block L2, Dutch continental shelf. In *Geology of Gas and Oil under the Netherlands* (pp. 159–166). Springer. https://doi.org/10.1007/978-94-009-0121-6_14

Edgar, L. A., Fedo, C. M., Gupta, S., Banham, S. G., Fraeman, A. A., Grotzinger, J. P., et al. (2020). A lacustrine paleoenvironment recorded at Vera Rubin Ridge, Gale crater: Overview of the sedimentology and stratigraphy observed by the Mars Science Laboratory Curiosity Rover. *Journal of Geophysical Research: Planets*, *125*(3), e2019JE006307. https://doi.org/10.1029/2019JE006307

Edgett, K. S. (2002). Low-albedo surfaces and eolian sediment: Mars Orbiter Camera views of western Arabia Terra craters and wind streaks. *Journal of Geophysical Research*, *107*(E6), 5-1–5-22. https://doi.org/10.1029/2001JE001587

Ehlmann, B. L., Mustard, J. F., Swayze, G. A., Clark, R. N., Bishop, J. L., Poulet, F., et al. (2009). Identification of hydrated silicate minerals on Mars using MRO-CRISM: Geologic context near Nili Fossae and implications for aqueous alteration. *Journal of Geophysical Research*, *114*(E2), E00D08. https://doi.org/10.1029/2009JE003339

Ehrlich, J., & Gross, C. (2020). *Morphologic mapping of Becquerel crater, Mars and comparison of light-toned layered deposit formation theories*. In *Paper presented at 51st Annual Lunar and Planetary Science Conference*. Abstract 1988.

Fawdon, P., Balme, M., Davis, J., Bridges, J., Gupta, S., & Quantin-Nataf, C. (2022). Rivers and lakes in Western Arabia Terra: The fluvial catchment of the ExoMars 2022 rover landing site. *Journal of Geophysical Research: Planets*, *127*(2), e2021JE007045. https://doi.org/10.1029/2021JE007045

Fergason, R. L., & Christensen, P. R. (2008). Formation and erosion of layered materials: Geologic and dust cycle history of eastern Arabia Terra, Mars. *Journal of Geophysical Research*, *113*(E12), E12001. https://doi.org/10.1029/2007JE002973

Flahaut, J., Carter, J., Poulet, F., Bibring, J. P., Van Westrenen, W., Davies, G. R., & Murchie, S. L. (2015). Embedded clays and sulfates in Meridiani Planum, Mars. *Icarus*, *248*, 269–288. https://doi.org/10.1016/j.icarus.2014.10.046

Franchi, F., Rossi, A. P., Pondrelli, M., & Cavalazzi, B. (2014). Geometry, stratigraphy and evidences for fluid expulsion within Crommelin crater deposits, Arabia Terra, Mars. *Planetary and Space Science*, *92*, 34–48. https://doi.org/10.1016/j.pss.2013.12.013

Fueten, F., Flahaut, J., Le Deit, L., Stesky, R., Hauber, E., & Gwinner, K. (2011). Interior layered deposits within a perched basin, southern Coprates Chasma, Mars: Evidence for their formation, alteration, and erosion. *Journal of Geophysical Research*, *116*(E2), E02003. https://doi.org/10.1029/2010JE003695

Fueten, F., Flahaut, J., Stesky, R., Hauber, E., & Rossi, A. P. (2014). Stratigraphy and mineralogy of Candor Mensa, West Candor Chasma, Mars: Insights into geologic history of Valles Marineris. *Journal of Geophysical Research: Planets*, *119*(2), 331–354. https://doi.org/10.1002/2013je004557

Fueten, F., Novakovic, N., Stesky, R., Flahaut, J., Hauber, E., & Rossi, A. P. (2017). The evolution of Juventae Chasma, Valles Marineris, Mars: Progressive collapse and sedimentation. *Journal of Geophysical Research: Planets*, *122*(11), 2223–2249. https://doi.org/10.1002/2017JE005334

Fueten, F., Racher, H., Stesky, R., MacKinnon, P., Hauber, E., McGuire, P. C., et al. (2010). Structural analysis of interior layered deposits in Northern Coprates Chasma, Mars. *Earth and Planetary Science Letters*, *294*(3–4), 343–356. https://doi.org/10.1016/j.epsl.2009.11.004

Fueten, F., Stesky, R., MacKinnon, P., Hauber, E., Gwinner, K., Scholten, F., et al. (2006). A structural study of an interior layered deposit in southwestern Candor Chasma, Valles Marineris, Mars, using high resolution stereo camera data from Mars Express. *Geophysical Research Letters*, *33*(7), L07202. https://doi.org/10.1029/2005GL025035

Fueten, F., Stesky, R., MacKinnon, P., Hauber, E., Zegers, T., Gwinner, K., et al. (2008). Stratigraphy and structure of interior layered deposits in west Candor Chasma, Mars, from High Resolution Stereo Camera (HRSC) stereo imagery and derived elevations. *Journal of Geophysical Research*, *113*(E10), E10008. https://doi.org/10.1029/2007JE003053

Fueten, F., Stesky, R. M., & MacKinnon, P. (2005). Structural attitudes of large scale layering in Valles Marineris, Mars, calculated from Mars Orbiter Laser Altimeter data and Mars Orbiter Camera imagery. *Icarus*, *175*(1), 68–77. https://doi.org/10.1016/j.icarus.2004.11.010

Gendrin, A., Mangold, N., Bibring, J.-P., Langevin, Y., Gondet, B., Poulet, F., et al. (2005). Sulfates in Martian layered terrains: The OMEGA/Mars Express view. *Science*, *307*(5715), 1587–1591. https://doi.org/10.1126/science.1109087

Golombek, M., Grant, J., Vasavada, A. R., Grotzinger, J., Watkins, M., Kipp, D., et al. (2011). *Final four landing sites for the Mars Science Laboratory*. In *Paper presented at 42nd Annual Lunar and Planetary Science Conference*. Abstract 1520.

Golombek, M. P., Anderson, F. S., & Zuber, M. T. (2001). Martian wrinkle ridge topography: Evidence for subsurface faults from MOLA. *Journal of Geophysical Research*, *106*(E10), 23811–23821. https://doi.org/10.1029/2000JE001308

Gou, S., Yue, Z., Di, K., & Wang, J. (2014). Hyperspectral identification of mineral diversity and formation mechanism analysis in the Mclaughlin crater on Mars. In *Remote Sensing of the Environment: 18th National Symposium on Remote Sensing of China* (Vol. 9158, pp. 110–115). SPIE.

Goudge, T. A., Milliken, R. E., Head, J. W., Mustard, J. F., & Fassett, C. I. (2017). Sedimentological evidence for a deltaic origin of the western fan deposit in Jezero crater, Mars and implications for future exploration. *Earth and Planetary Science Letters*, *458*, 357–365. https://doi.org/10.1016/j.epsl.2016.10.056

Grant, J. A., Golombek, M. P., Grotzinger, J. P., Wilson, S. A., Watkins, M. M., Vasavada, A. R., et al. (2011). The science process for selecting the landing site for the 2011 Mars Science Laboratory. *Planetary and Space Science*, *59*(11–12), 1114–1127. https://doi.org/10.1016/j.pss.2010.06.016

Grindrod, P. M., & Balme, M. R. (2010). Groundwater processes in Hebes Chasma, Mars. *Geophysical Research Letters*, *37*(13), L13202. https://doi.org/10.1029/2010gl044122

Grotzinger, J. P., Sumner, D. Y., Kah, L. C., Stack, K., Gupta, S., Edgar, L., et al. (2014). A habitable fluvio-lacustrine environment at Yellowknife Bay, Gale Crater, Mars. *Science*, *343*(6169), 1242777. https://doi.org/10.1126/science.1242777

Head, J. W., & Mustard, J. F. (2006). Breccia dikes and crater-related faults in impact craters on Mars: Erosion and exposure on the floor of a crater 75 km in diameter at the dichotomy boundary. *Meteoritics & Planetary Science*, *41*(10), 1675–1690. https://doi.org/10.1111/j.1945-5100.2006.tb00444.x

Heather, D., Barthelemy, M., Manaud, N., Martinez, S., Szumlas, M., Vazquez, J., & Osuna, P. (2013a). *ESA's planetary science archive: Status, activities and plans*. *European Planetary Science Congress* (Vol. 8).

Heather, D., Barthelemy, M., Manaud, N., Martinez, S., Szumlas, M., Vazquez, J. L., et al. (2013b). *ESA's planetary science archive: Status and plans*. In *EGU General Assembly Conference Abstracts* (pp. EGU2013–9151).

Hodgson, R. A. (1961). Classification of structures on joint surfaces. *American Journal of Science*, *259*(7), 493–502. https://doi.org/10.1306/0BDA6278-16BD-11D7-8645000102C1865D

Hungr, O., Leroueil, S., & Picarelli, L. (2014). The Varnes classification of landslide types, an update. *Landslides*, *11*(2), 167–194. https://doi.org/10.1007/s10346-013-0436-y

Hunt, G. R. (1970). Visible and near-infrared spectra of minerals and rocks: I silicate minerals. *Modern Geology*, *1*, 283–300.

Hynek, B. M., Phillips, R. J., & Arvidson, R. E. (2003). Explosive volcanism in the Tharsis region: Global evidence in the Martian geologic record. *Journal of Geophysical Research*, *108*(E9), 5111. https://doi.org/10.1029/2003JE002062

Jackson, M. P. A., Adams, J. B., Dooley, T. P., Gillespie, A. R., & Montgomery, D. R. (2011). Modeling the collapse of Hebes Chasma, Valles Marineris, Mars. *GSA Bulletin*, *123*(7–8), 1596–1627. https://doi.org/10.1130/B30307.1

Jaumann, R., Neukum, G., Behnke, T., Duxbury, T. C., Eichentopf, K., Flohrer, J., et al. (2007). The high-resolution stereo camera (HRSC) experiment on Mars Express: Instrument aspects and experiment conduct from interplanetary cruise through the nominal mission. *Planetary and Space Science*, *55*(7–8), 928–952. https://doi.org/10.1016/j.pss.2006.12.003

Kite, E. S., Lewis, K. W., Lamb, M. P., Newman, C. E., & Richardson, M. I. (2013). Growth and form of the mound in Gale Crater, Mars: Slope wind enhanced erosion and transport. *Geology*, *41*(5), 543–546. https://doi.org/10.1130/G33909.1

Koeberl, C., Reimold, W. U., & Brandi, D. (1996). Red Wing Creek structure, North Dakota: Petrographical and geochemical studies, and confirmation of impact origin. *Meteoritics & Planetary Science*, *31*(3), 335–342. https://doi.org/10.1111/j.1945-5100.1996.tb02070.x

Koeppel, A. H., Edwards, C. S., Annex, A. M., Lewis, K. W., & Carrillo, G. J. (2022). A fragile record of fleeting water on Mars. *Geology*, *50*(2), 152–157. https://doi.org/10.1130/g49285.1

Kokaly, R. F., Clark, R. N., Swayze, G. A., Livo, K. E., Hoefen, T. M., Pearson, N. C., et al. (2017). *USGS spectral library version 7* (Vol. 1035). US Geological Survey.

Kopf, A. J. (2002). Significance of mud volcanism. *Reviews of Geophysics*, *40*(2), 2–1. https://doi.org/10.1029/2000RG000093

Lakdawalla, E. (2019). Similarities and differences in the landing sites of ESA's and NASA's 2020 Mars rovers. *Nature Astronomy*, *3*(3), 190–192. https://doi.org/10.1038/s41550-019-0727-x

Lewis, K. W., & Aharonson, O. (2014). Occurrence and origin of rhythmic sedimentary rocks on Mars. *Journal of Geophysical Research: Planets*, *119*(6), 1432–1457. https://doi.org/10.1002/2013JE004404

Lewis, K. W., Aharonson, O., Grotzinger, J. P., Kirk, R. L., McEwen, A. S., & Suer, T. A. (2008). Quasi-periodic bedding in the sedimentary rock record of Mars. *Science*, *322*(5907), 1532–1535. https://doi.org/10.1126/science.1161870

Loizeau, D., Mangold, N., Poulet, F., Ansan, V., Hauber, E., Bibring, J. P., et al. (2010). Stratigraphy in the Mawrth Vallis region through OMEGA, HRSC color imagery and DTM. *Icarus*, *205*(2), 396–418. https://doi.org/10.1016/j.icarus.2009.04.018

Loizeau, D., Mangold, N., Poulet, F., Bibring, J. P., Bishop, J. L., Michalski, J., & Quantin, C. (2015). History of the clay-rich unit at Mawrth Vallis, Mars: High-resolution mapping of a candidate landing site. *Journal of Geophysical Research: Planets*, *120*(11), 1820–1846. https://doi.org/10.1002/2015JE004894

Loizeau, D., Werner, S. C., Mangold, N., Bibring, J. P., & Vago, J. L. (2012). Chronology of deposition and alteration in the Mawrth Vallis region, Mars. *Planetary and Space Science*, *72*(1), 31–43. https://doi.org/10.1016/j.pss.2012.06.023

Lucchitta, B. K. (1990). Young volcanic deposits in the Valles Marineris, Mars? *Icarus*, *86*(2), 476–509. https://doi.org/10.1016/0019-1035(90)90230-7

Lucchitta, B. K. (2010). Lakes in Valles Marineris. In N. A. Cabrol & E. A. Grin (Eds.), *Lakes on Mars* (p. 111). Elsevier.

Lucchitta, B. K., Isbell, N. K., & Howington-Kraus, A. (1994). Topography of Valles Marineris: Implications for erosional and structural history. *Journal of Geophysical Research*, *99*(E2), 3783–3798. https://doi.org/10.1029/93JE03095

Lucchitta, B. K., McEwen, A. S., Clow, G. D., Geissler, P. E., Singer, R. B., Schultz, R. A., & Squyres, S. W. (1992). The canyon system on Mars. *Mars* (pp. 453–492).

Malin, M. C. (2007). MRO context camera experiment data record level 0 v1.0 [Data set]. NASA Planetary Data System. https://doi.org/10.17189/1520266

Malin, M. C., Bell, J. F., III, Cantor, B. A., Caplinger, M. A., Calvin, W. M., Clancy, R. T., et al. (2007). Context camera investigation on board the Mars Reconnaissance Orbiter. *Journal of Geophysical Research*, *112*(E5), E05S04. https://doi.org/10.1029/2006je002808

Malin, M. C., & Edgett, K. S. (2000). Sedimentary rocks of early Mars. *Science*, *290*(5498), 1927–1937. https://doi.org/10.1126/science.290.5498.1927

Mangold, N., Ansan, V., Masson, P., & Vincendon, C. (2009). Estimate of aeolian dust thickness in Arabia Terra, Mars: Implications of a thick mantle (>20 m) for hydrogen detection. *Géomorphologie: Relief, Processus, Environnement*, *15*(1), 23–32. https://doi.org/10.4000/geomorphologie.7472

Mangold, N., Gendrin, A., Gondet, B., LeMouelic, S., Quantin, C., Ansan, V., et al. (2008). Spectral and geological study of the sulfate-rich region of West Candor Chasma, Mars. *Icarus*, *194*(2), 519–543. https://doi.org/10.1016/j.icarus.2007.10.021

Masson, D. G., Harbitz, C. B., Wynn, R. B., Pedersen, G., & Løvholt, F. (2006). Submarine landslides: Processes, triggers and hazard prediction. *Philosophical Transactions of the Royal Society A: Mathematical, Physical & Engineering Sciences*, *364*(1845), 2009–2039. https://doi.org/10.1098/rsta.2006.1810

McEwen, A. (2006). *The high resolution imaging science experiment (HiRISE) on Mars reconnaissance orbiter (MRO)*. In *36th COSPAR Scientific Assembly* (Vol. 36, p. 1096).

McEwen, A., Eliason, E., Bergstrom, J., Bridges, N., Hansen, C., Delamere, W. A., et al. (2005). *MRO's high resolution imaging science experiment (HiRISE)*. *AGU Fall Meeting Abstracts* (Vol. 2005, pp. P23A–0171).

McEwen, A. S., Eliason, E. M., Bergstrom, J. W., Bridges, N. T., Hansen, C. J., Delamere, W. A., et al. (2007). Mars Reconnaissance Orbiter's high resolution imaging science experiment (HiRISE). *Journal of Geophysical Research*, *112*(E5), E05S02. https://doi.org/10.1029/2005je002605

McEwen, A. S., & Team, H. (2009). *Recent MRO/HiRISE Discoveries on Mars*. In *EGU General Assembly Conference Abstracts* (p. 6434).

McGill, G. E. (2000). Crustal history of north central Arabia Terra, Mars. *Journal of Geophysical Research*, *105*(E3), 6945–6959. https://doi.org/10.1029/1999JE001175

McGuire, P. C., Bishop, J. L., Brown, A. J., Fraeman, A. A., Marzo, G. A., Morgan, M. F., et al. (2009). An improvement to the volcano-scan algorithm for atmospheric correction of CRISM and OMEGA spectral data. *Planetary and Space Science*, *57*(7), 809–815. https://doi.org/10.1016/j.pss.2009.03.007

McLennan, S. M., Bell, J. F., III, Calvin, W. M., Christensen, P. R., Clark, B. D., De Souza, P. A., et al. (2005). Provenance and diagenesis of the evaporite-bearing Burns formation, Meridiani Planum, Mars. *Earth and Planetary Science Letters*, *240*(1), 95–121. https://doi.org/10.1016/j.epsl.2005.09.041

Michalski, J., & Niles, P. B. (2012). Atmospheric origin of Martian interior layered deposits: Links to climate change and the global sulfur cycle. *Geology*, *40*(5), 419–422. https://doi.org/10.1130/G32971.1

Michalski, J. R., & Bleacher, J. E. (2013). Supervolcanoes within an ancient volcanic province in Arabia Terra, Mars. *Nature*, *502*(7469), 47–52. https://doi.org/10.1038/nature12482

Michalski, J. R., Cuadros, J., Niles, P. B., Parnell, J., Rogers, A. D., & Wright, S. P. (2013). Groundwater activity on Mars and implications for a deep biosphere. *Nature Geoscience*, *6*(2), 133–138. https://doi.org/10.1038/ngeo1706

Michalski, J. R., Glotch, T. D., Rogers, A. D., Niles, P. B., Cuadros, J., Ashley, J. W., & Johnson, S. S. (2019). The geology and astrobiology of McLaughlin Crater, Mars: An ancient lacustrine basin containing turbidites, mudstones, and serpentinites. *Journal of Geophysical Research: Planets*, *124*(4), 910–940. https://doi.org/10.1029/2018JE005796

Michalski, J. R., & Niles, P. B. (2010). Deep crustal carbonate rocks exposed by meteor impact on Mars. *Nature Geoscience*, *3*(11), 751–755. https://doi.org/10.1038/ngeo971

Michalski, J. R., Niles, P. B., Cuadros, J., & Baldridge, A. M. (2013). Multiple working hypotheses for the formation of compositional stratigraphy on Mars: Insights from the Mawrth Vallis region. *Icarus*, *226*(1), 816–840. https://doi.org/10.1016/j.icarus.2013.05.024

Milliken, R. E., Grotzinger, J. P., & Thomson, B. J. (2010). Paleoclimate of Mars as captured by the stratigraphic record in Gale Crater. *Geophysical Research Letters*, *37*(4). https://doi.org/10.1029/2009GL041870

Milliken, R. E., Swayze, G. A., Arvidson, R. E., Bishop, J. L., Clark, R. N., Ehlmann, B. L., et al. (2008). Opaline silica in young deposits on Mars. *Geology*, *36*(11), 847–850. https://doi.org/10.1130/G24967A.1

Molina, A., López, I., Prieto-Ballesteros, O., Fernández-Remolar, D., de Pablo, M. Á., & Gómez, F. (2017). Coogoon Valles, western Arabia Terra: Hydrological evolution of a complex Martian channel system. *Icarus*, *293*, 27–44. https://doi.org/10.1016/j.icarus.2017.04.002

Moratto, Z. M., Broxton, M. J., Beyer, R. A., Lundy, M., & Husmann, K. (2010). Ames Stereo Pipeline, NASA's open source automated stereogrammetry software. *Lunar and Planetary Science Conference*, *1533*, 2364.

Morley, C. K., & Guerin, G. (1996). Comparison of gravity-driven deformation styles and behavior associated with mobile shales and salt. *Tectonics*, *15*(6), 1154–1170. https://doi.org/10.1029/96TC01416

Murana, A. (2018). Geology of Danielson Crater, Mars. *Journal of Maps*, *14*(2), 161–172. https://doi.org/10.1080/17445647.2018.1443029

Murchie, S., Arvidson, R., Bedini, P., Beisser, K., Bibring, J. P., Bishop, J., et al. (2007). Compact reconnaissance imaging spectrometer for Mars (CRISM) on Mars Reconnaissance Orbiter (MRO). *Journal of Geophysical Research: Planets*, *112*(E5), E05S03. https://doi.org/10.1029/2006je002682

Murchie, S. L., Mustard, J. F., Ehlmann, B. L., Milliken, R. E., Bishop, J. L., McKeown, N. K., et al. (2009). A synthesis of Martian aqueous mineralogy after 1 Mars year of observations from the Mars Reconnaissance Orbiter. *Journal of Geophysical Research: Planets*, *114*(E2), E00D06. https://doi.org/10.1029/2009JE003342

Neukum, G., & Jaumann, R. (2004). *HRSC: The high resolution stereo camera of Mars Express*. In *Mars Express: The scientific payload* (Vol. 1240, pp. 17–35).

Niles, P. B., & Michalski, J. (2009). Meridiani Planum sediments on Mars formed through weathering in massive ice deposits. *Nature Geoscience*, *2*(3), 215–220. https://doi.org/10.1038/ngeo438

Noe Dobrea, E. Z., Michalski, J., & Swayze, G. (2011). Aqueous mineralogy and stratigraphy at and around the proposed Mawrth Vallis MSL Landing Site: New insights into the aqueous history of the region. *Mars*, *6*, 32–46. https://doi.org/10.1555/mars.2011.0003

Noel, A., Bishop, J. L., Al-Samir, M., Gross, C., Flahaut, J., McGuire, P. C., et al. (2015). Mineralogy, morphology and stratigraphy of the light-toned interior layered deposits at Juventae Chasma. *Icarus*, *251*, 315–331. https://doi.org/10.1016/j.icarus.2014.09.033

Oehler, D. Z., & Allen, C. C. (2010). Evidence for pervasive mud volcanism in Acidalia Planitia, Mars. *Icarus*, *208*(2), 636–657. https://doi.org/10.1016/j.icarus.2010.03.031

Okubo, C. H. (2014). *Bedrock geologic and structural map through the western Candor Colles Region of Mars* (Vol. 3309) US Geological Survey Scientific Investigations Map.

Okubo, C. H., Schultz, R. A., Chan, M. A., Komatsu, G., & High-Resolution Imaging Science Experiment (HiRISE) Team. (2009). Deformation band clusters on Mars and implications for subsurface fluid flow. *The Geological Society of America Bulletin*, *121*(3–4), 474–482. https://doi.org/10.1130/B26421.1

Osinski, G. R., Lee, P., Parnell, J., Spray, J. G., & Baron, M. (2005). A case study of impact-induced hydrothermal activity: The Haughton impact structure, Devon Island, Canadian High Arctic. *Meteoritics & Planetary Science*, *40*(12), 1859–1877. https://doi.org/10.1111/j.1945-5100.2005.tb00150.x

Osinski, G. R., & Spray, J. G. (2005). Tectonics of complex crater formation as revealed by the Haughton impact structure, Devon Island, Canadian High Arctic. *Meteoritics & Planetary Science*, *40*(12), 1813–1834. https://doi.org/10.1111/j.1945-5100.2005.tb00148.x

Pajola, M., Pozzobon, R., Silvestro, S., Salese, F., Rossato, S., Pompilio, L., et al. (2022). Geology, in-situ resource-identification and engineering analysis of the vernal crater area (Arabia Terra): A suitable Mars human landing site candidate. *Planetary and Space Science*, *213*, 105444. https://doi.org/10.1016/j.pss.2022.105444

Pangaea Scientific. (2011). *Orion: Orientation Hunter* [Computer software]. *Supported by Canada Centre for Remote Sensing, Natural Resources Canada*.

Pondrelli, M., Rossi, A. P., Le Deit, L., Fueten, F., van Gasselt, S., Glamoclija, M., et al. (2015). Equatorial layered deposits in Arabia Terra, Mars: Facies and process variability. *Bulletin*, *127*(7–8), 1064–1089.

Pondrelli, M., Rossi, A. P., Le Deit, L., Schmidt, G. W., Pozzobon, R., Hauber, E., & Salese, F. (2019). Groundwater control and process variability on the equatorial layered deposits of Kotido Crater, Mars. *Journal of Geophysical Research: Planets*, *124*(3), 779–800. https://doi.org/10.1029/2018je005656

Pondrelli, M., Rossi, A. P., Ori, G. G., Van Gasselt, S., Praeg, D., & Ceramicola, S. (2011). Mud volcanoes in the geologic record of Mars: The case of Firsoff crater. *Earth and Planetary Science Letters*, *304*(3–4), 511–519. https://doi.org/10.1016/j.epsl.2011.02.027

Popa, C., Esposito, F., & Colangeli, L. (2008). *Becquerel crater deposit on Mars, a case of namakier diapirism?* In *Paper presented at 39th Annual Lunar and Planetary Science Conference*. Abstract 1623.

Poulet, F., Arvidson, R. E., Gomez, C., Morris, R. V., Bibring, J. P., Langevin, Y., et al. (2008). Mineralogy of Terra Meridiani and western Arabia Terra from OMEGA/MEx and implications for their formation. *Icarus*, *195*(1), 106–130. https://doi.org/10.1016/j.icarus.2007.11.031

Pozzobon, R., Mazzarini, F., Massironi, M., Rossi, A. P., Pondrelli, M., Cremonese, G., & Marinangeli, L. (2019). Fluids mobilization in Arabia Terra, Mars: Depth of pressurized reservoir from mounds self-similar clustering. *Icarus*, *321*, 938–959. https://doi.org/10.1016/j.icarus.2018.12.023

Price, N. J., & Cosgrove, J. W. (1990). *Analysis of geological structures*. Cambridge University Press.

Quantin, C., Mangold, N., Hauber, E., Flahaut, J., Le Deit, L., Fueten, F., et al. (2010). *Timing constraints of interior layered deposit emplacement in Valles Marineris*. In *First International Conference on Mars Sedimentology and Stratigraphy* (Vol. 6048).

Quantin-Nataf, C., Carter, J., Mandon, L., Thollot, P., Balme, M., Volat, M., et al. (2021). Oxia Planum: The landing site for the ExoMars "Rosalind Franklin" rover mission: Geological context and prelanding interpretation. *Astrobiology*, *21*(3), 345–366. https://doi.org/10.1089/ast.2019.2191

Rampe, E. B., Ming, D. W., Blake, D. F., Bristow, T. F., Chipera, S. J., Grotzinger, J. P., et al. (2017). Mineralogy of an ancient lacustrine mudstone succession from the Murray formation, Gale crater, Mars. *Earth and Planetary Science Letters*, *471*, 172–185. https://doi.org/10.1016/j.epsl.2017.04.021

Rivera-Hernández, F., Sumner, D. Y., Mangold, N., Banham, S. G., Edgett, K. S., Fedo, C. M., et al. (2020). Grain size variations in the Murray formation: Stratigraphic evidence for changing depositional environments in Gale crater, Mars. *Journal of Geophysical Research: Planets*, *125*(2), e2019JE006230. https://doi.org/10.1029/2019JE006230

Roach, L. H., Mustard, J. F., Lane, M. D., Bishop, J. L., & Murchie, S. L. (2010). Diagenetic haematite and sulfate assemblages in Valles Marineris. *Icarus*, *207*(2), 659–674. https://doi.org/10.1016/j.icarus.2009.11.029

Roach, L. H., Mustard, J. F., Swayze, G., Milliken, R. E., Bishop, J. L., Murchie, S. L., & Lichtenberg, K. (2010). Hydrated mineral stratigraphy of Ius Chasma, Valles Marineris. *Icarus*, *206*(1), 253–268. https://doi.org/10.1016/j.icarus.2009.09.003

Rodriguez, J. A. P., Fairén, A. G., Tanaka, K. L., Zarroca, M., Linares, R., Platz, T., et al. (2016). Tsunami waves extensively resurfaced the shorelines of an early Martian ocean. *Scientific Reports*, *6*(1), 1–8. https://doi.org/10.1038/srep25106

Rossi, A. P., Neukum, G., Pondrelli, M., Van Gasselt, S., Zegers, T., Hauber, E., et al. (2008). Large-scale spring deposits on Mars? *Journal of Geophysical Research*, *113*(E8), E08016. https://doi.org/10.1029/2007je003062

Rossi, A. P., Pondrelli, M., Hauber, E., Baliva, A., Michael, G., Ori, G. G., et al. (2009). *Stratigraphic architecture and structural control on sediment emplacement in Becquerel crater (Mars)*. In *Paper presented at 40th Annual Lunar and Planetary Science Conference*. Abstract 1588.

Ruff, S. W., Farmer, J. D., Calvin, W. M., Herkenhoff, K. E., Johnson, J. R., Morris, R. V., et al. (2011). Characteristics, distribution, origin, and significance of opaline silica observed by the Spirit rover in Gusev crater, Mars. *Journal of Geophysical Research*, *116*(E7), E00F23. https://doi.org/10.1029/2010JE003767

Ruj, T., Komatsu, G., Dohm, J. M., Miyamoto, H., & Salese, F. (2017). Generic identification and classification of morphostructures in the Noachis-Sabaea region, southern highlands of Mars. *Journal of Maps*, *13*(2), 755–766. https://doi.org/10.1080/17445647.2017.1379913

Salese, F., McMahon, W. J., Balme, M. R., Ansan, V., Davis, J. M., & Kleinhans, M. G. (2020). Sustained fluvial deposition recorded in Mars' Noachian stratigraphic record. *Nature Communications*, *11*(1), 1–8. https://doi.org/10.1038/s41467-020-15622-0

Salese, F., Pondrelli, M., Neeseman, A., Schmidt, G., & Ori, G. G. (2019). Geological evidence of planet-wide groundwater system on Mars. *Journal of Geophysical Research: Planets*, *124*(2), 374–395. https://doi.org/10.1029/2018JE005802

Schmidt, G. (2022). Layer thicknesses, layer attitudes, CRISM, and DTMs of Becquerel Crater [Dataset]. Zenodo. https://doi.org/10.5281/zenodo.6560965

Schmidt, G., Fueten, F., Stesky, R., Flahuat, J., & Hauber, E. (2018). Geology of Hebes Chasma, Mars: 1. Structure, stratigraphy, and mineralogy of the interior layered deposits. *Journal of Geophysical Research: Planets*, *123*(11), 2893–2919. https://doi.org/10.1029/2018JE005658

Schmidt, G., Pondrelli, M., Salese, F., Rossi, A. P., Le Deit, L., Fueten, F., & Salvini, F. (2021). Depositional Controls of the Layered Deposits of Arabia Terra, Mars: Hints From Basin Geometries and Stratigraphic Trends. *Journal of Geophysical Research: Planets*, *126*(11). https://doi.org/10.1029/2021je006974

Schultz, R. A. (1998). Multiple-process origin of Valles Marineris basins and troughs, Mars. *Planetary and Space Science*, *46*(6–7), 827–834. https://doi.org/10.1016/S0032-0633(98)00030-0

Shirozu, H., & Bailey, S. W. (1966). Crystal structure of a two-layer Mg-vermiculite. *American Mineralogist: Journal of Earth and Planetary Materials*, *51*(7), 1124–1143.

Skempton, A. W., & Petley, D. J. (1967). *The strength along structural discontinuities in stiff clays*. In *Proceedings of the Geotechnical Conference at Oslo, Norway* (Vol. 2, p. 153).

Squyres, S. W., Arvidson, R. E., Bell, J. F., Brückner, J., Cabrol, N. A., Calvin, W., et al. (2004). The Opportunity Rover's Athena Science Investigation at Meridiani Planum, Mars. *Science*, *306*(5702), 1698–1703. https://doi.org/10.1126/science.1106171

Squyres, S. W., Grotzinger, J. P., Arvidson, R. E., Bell, J. F., III, Calvin, W., Christensen, P. R., et al. (2004). In situ evidence for an ancient aqueous environment at Meridiani Planum, Mars. *Science*, *306*(5702), 1709–1714. https://doi.org/10.1126/science.1104559

Sun, V. Z., & Milliken, R. E. (2018). Distinct geologic settings of opal-A and more crystalline hydrated silica on Mars. *Geophysical Research Letters*, *45*(19), 10–221. https://doi.org/10.1029/2018GL078494

Sunwall, M. T., McQuillan, K. A., & Nick, C. J. (1983). Salt Diapir–Gulf of Mexico. Studies in Geology 15, Volume 2: Seismic Expression of Structural Styles: A Picture and Work Atlas, *American Association of Petroleum Geologists*.

Sutton, S., Chojnacki, M., Kilgallon, A., & Team, H. (2015). *Precision and accuracy of simultaneously collected HiRISE digital terrain models*. In *46th Annual Lunar and Planetary Science Conference*. Abstract 3010.

Tanaka, K. L., Skinner, J. A., Jr., Dohm, J. M., Irwin, R. P., III, Kolb, E. J., Fortezzo, C. M., et al. (2014). Geologic map of Mars: U.S. *Geological Survey Scientific Investigations Map 3292, scale 1:20, 000, 000, pamphlet* (p. 43). https://doi.org/10.3133/sim3292

Thomson, B. J., Bridges, N. T., Milliken, R., Baldridge, A., Hook, S. J., Crowley, J. K., et al. (2011). Constraints on the origin and evolution of the layered mound in Gale Crater, Mars using Mars Reconnaissance Orbiter data. *Icarus*, *214*(2), 413–432. https://doi.org/10.1016/j.icarus.2011.05.002

Urso, A., Chojnacki, M., & Vaz, D. A. (2018). Dune-Yardang interactions in Becquerel Crater, Mars. *Journal of Geophysical Research: Planets*, *123*(2), 353–368. https://doi.org/10.1002/2017JE005465

Vago, J., Witasse, O., Svedhem, H., Baglioni, P., Haldemann, A., Gianfiglio, G., et al. (2015). ESA ExoMars program: The next step in exploring Mars. *Solar System Research*, *49*(7), 518–528. https://doi.org/10.1134/S0038094615070199

Vago, J. L., Westall, F., Coates, A. J., Jaumann, R., Korablev, O., Ciarletti, V., et al. (2017). Habitability on early Mars and the search for biosignatures with the ExoMars Rover. *Astrobiology*, *17*(6–7), 471–510. https://doi.org/10.1089/ast.2016.1533

Varnes, D. J. (1978). Slope movement types and processes. *Special Report*, *176*, 11–33.

Viviano-Beck, C. E., Seelos, F. P., Murchie, S. L., Kahn, E. G., Seelos, K. D., Taylor, H. W., et al. (2014). Revised CRISM spectral parameters and summary products based on the currently detected mineral diversity on Mars. *Journal of Geophysical Research: Planets*, *119*(6), 1403–1431. https://doi.org/10.1002/2014JE004627

Wang, A., Jolliff, B. L., Liu, Y., & Connor, K. (2016). Setting constraints on the nature and origin of the two major hydrous sulfates on Mars: Monohydrated and polyhydrated sulfates. *Journal of Geophysical Research: Planets*, *121*(4), 678–694. https://doi.org/10.1002/2015JE004889

Warren, J. K. (2010). Evaporites through time: Tectonic, climatic and eustatic controls in marine and nonmarine deposits. *Earth-Science Reviews*, *98*(3–4), 217–268. https://doi.org/10.1016/j.earscirev.2009.11.004

Warren, J. K. (2016). *Evaporites: A geological compendium*. Springer. https://doi.org/10.1007/978-3-319-39193-9_100-1

Watters, T. R. (2003). Thrust faults along the dichotomy boundary in the eastern hemisphere of Mars. *Journal of Geophysical Research*, *108*(E6), 5054. https://doi.org/10.1029/2002JE001934

Webb, V. E. (2004). Putative shorelines in northern Arabia Terra, Mars. *Journal of Geophysical Research*, *109*(E9), E09010. https://doi.org/10.1029/2003JE002205

Westall, F., Edwards, H. G., Whyte, L., Fairén, A. G., Bibring, J. P., Bridges, J., et al. (2014). *Recommendation for the narrowing of ExoMars 2018 landing site [R]. Technical Report EXM-SCI-LSS-ESA/IKI-004*. European Space Agency.

Whelley, P., Novak, A. M., Richardson, J., Bleacher, J., Mach, K., & Smith, R. N. (2021). Stratigraphic evidence for early Martian explosive volcanism in Arabia Terra. *Geophysical Research Letters*, *48*(15), e2021GL094109. https://doi.org/10.1029/2021GL094109

Wray, J. J. (2013). Gale Crater: The Mars Science Laboratory/Curiosity rover landing site. *International Journal of Astrobiology*, *12*(1), 25–38. https://doi.org/10.1017/S1473550412000328

Wray, J. J., Ehlmann, B. L., Squyres, S. W., Mustard, J. F., & Kirk, R. L. (2008). Compositional stratigraphy of clay-bearing layered deposits at Mawrth Vallis, Mars. *Geophysical Research Letters*, *35*(12). https://doi.org/10.1029/2008GL034385

Ye, Y. C. (2017). *Marine geo-hazards in China*. Elsevier. https://doi.org/10.1016/B978-0-12-812726-1.00006-1

Zabrusky, K., Andrews-Hanna, J. C., & Wiseman, S. M. (2012). Reconstructing the distribution and depositional history of the sedimentary deposits of Arabia Terra, Mars. *Icarus*, *220*(2), 311–330. https://doi.org/10.1016/j.icarus.2012.05.007